Atmospheric Research 163 (2015) 74–90

Contents lists available at ScienceDirect

Atmospheric Research

journal homepage: www.elsevier.com/locate/atmos

The oceanic shipboard precipitation measurement network for surface validation — OceanRAIN ☆

Christian Klepp *

Universität Hamburg, CliSAP/CEN, Initiative Pro Klima, Bundesstraße 55, 20146 Hamburg, Germany

ARTICLE INFO

Article history:
Received 21 February 2014
Received in revised form 26 September 2014
Accepted 24 December 2014
Available online 8 January 2015

Keywords:
Precipitation
Oceanic measurements
Optical disdrometer
In-situ validation
Satellite
Snow

ABSTRACT

Systematic high quality oceanic in-situ precipitation measurements are requested on an international science level and are essential for improved understanding and validation of hydrological processes in satellite, re-analysis and model data. OceanRAIN, the shipboard "Ocean Rainfall And Ice-phase precipitation measurement Network" for surface validation is, to date, the only systematic long-term disdrometer-based oceanic shipboard precipitation data collection effort to establish a comprehensive statistical basis of precipitation for all climate related hotspots over the global oceans. OceanRAIN utilizes automated disdrometer systems (ODM470) capable of measuring precipitation occurrence, intensity and accumulation and discriminates for rain, snow and mixed-phase precipitation through minute-based particle size distributions. The ODM470 was especially designed for shipboard operation under high and frequently varying wind speeds and rough sea states. This paper provides an overview on the OceanRAIN project, the instrumentation, algorithms, methodology, and data products. The procedure of the data processing chain is outlined, including calibration, shipboard operation, data ingest and quality control. The selected research ships do not circumvent high impact weather, allowing for a collection of the full precipitation spectrum including extremes. By October 2014 the fast growing OceanRAIN database comprised more than 3.7 million minutes of precipitation measurements (including true zeros) since its start in 2010. OceanRAIN aims at increasing knowledge about oceanic precipitation, improving error characterization of GPM (Global Precipitation Measurement) era precipitation retrievals, adding to the continual improvement of the satellite retrieval algorithms, as well as benchmarking existing satellite-based climatologies, re-analysis and model data. The accumulating data volume can be utilized for statistical and process study applications on different temporal and spatial scales, microphysical studies of rain and snow formation, and yields insight to the point-to-area problem of precipitation. Information on OceanRAIN including data products is available via http://www.oceanrain.org.

1. Introduction

Precipitation is one of the key air–sea flux parameters and a fundamental component of the Earth's hydrological and energy cycle. Thus, the precipitation flux is among the essential climate variables for understanding and modeling the climate system (Oki, 1999; Trenberth et al., 2009). The water cycle is to a large extent driven by, and feeds back onto, the global ocean. The Intergovernmental Panel on Climate Change (IPCC, 2013) reports on global-scale changes in precipitation patterns over land and changes in surface and subsurface ocean salinity. These are linked to changes in evaporation and precipitation over the oceans. It is also noted that precipitation estimates are hampered by observational uncertainties. Moreover, precipitation is among the most intermittent and inhomogeneous meteorological parameters with high spatio-temporal variability and occurs in liquid, solid and mixed-phases. Consequently, measuring precipitation is notoriously difficult resulting in large uncertainties (Weller et al., 2008). The balance between precipitation and evaporation results in the freshwater flux, which is an important driver for ocean mixing and circulation (Wijesekera et al., 2005). Besides evaporation, more realistic precipitation observations also improve the freshwater flux estimates. Hence, understanding oceanic precipitation patterns is essential for surface water density, stratification, and mixing. The closure of upper ocean heat and freshwater budgets require high quality precipitation information (Romanova et al., 2010).

Measurements of precipitation over the ocean with adequate sampling largely improved with the advent of passive and active microwave remote sensing from space (Kidd and Huffman, 2011). Nonetheless, satellite-based climatologies use different retrieval techniques and approaches to derive the precipitation parameter, causing a large range of estimates among the available products (e.g. GPCP (Huffman et al., 1997), TMPA (Huffman et al., 2007), HOAPS (Andersson et al., 2010) and others). Furthermore, these climatologies do not discriminate between liquid and solid precipitation. Detection of snowfall and mixed-

☆ OceanRAIN, Ocean Rainfall And Ice-phase precipitation measurement Network.

* Tel.: +49 4041173353.
E-mail address: christian.klepp@zmaw.de.

http://dx.doi.org/10.1016/j.atmosres.2014.12.014
0169-8095/

phase precipitation from space remains a challenging task (Levizzani et al., 2011). The Cloud Profiling Radar (CPR) on Cloudsat is capable of identifying and retrieving both rainfall and snowfall, and, in particular, light to very light precipitation (Ellis et al., 2009; Mitrescu et al., 2010). Evaluation studies of these satellite, re-analysis and model climatologies exhibit large differences among each other, especially for light rainfall and high-latitude cold-season precipitation (Petty, 1997; Béranger et al., 2006; Andersson et al., 2011; Stephens et al., 2012). Errors, biases and uncertainties of satellite data sets remain obscured as oceanic surface validation data is not available. It is therefore of essential importance to understand their accuracy and limitations. This holds especially true for the new sensor generation of SSMIS (Special Sensor Microwave Imager Sounder) and the GPM (Global Precipitation Measurement) era constellation aiming at 3-hourly global products of precipitation. Due to the lack of oceanic precipitation surface validation data within GPM-GV (Global Precipitation Measurement — Ground Validation; Hou et al., 2014), coastal and island-based radar sites are used. The radars are calibrated using gauges and drop size distributions from land- and island-based disdrometers. However, the backscattered radiation is dependent upon the drop size distribution. As algorithm retrieval errors have a strong dependence on the meteorological regime, this calibration is not overly representative for precipitation in remote ocean areas (Anagnostou et al., 1999). Furthermore, coastlines and islands may orographically or thermodynamically influence local precipitation, adding to the non-representativeness.

In summary, these deficits call for high quality in-situ validation data of precipitation. Over land these are collected through radar networks (Kidd and Huffman, 2011) and rain gauges (GPCC, Global Precipitation Climatology Center; Schneider et al., 2013). In contrast, the global ocean, covering about 71% of Earth's surface, is almost void of quantitative precipitation surface reference data (Adler et al., 2012). Manual weather observations in the form of reports from Voluntary Observing Ships (VOS; Kent et al., 2010) as well as automated underway rain gauge measurements onboard research, merchant and cruise ships (Smith et al., 2010; Bumke et al., 2012) in combination with tropical buoy gauge arrays (Hayes et al., 1991; Bourlès et al., 2008) have been used in most recent ship based estimates of precipitation (e.g. Atlas of Surface Marine Data (da Silva et al., 1994); SOC (Josey et al., 1998); ICOADS (Woodruff et al., 2011), NOCS (Berry and Kent, 2011); OceanSITES (Send et al., 2010) and SAMOS (Smith et al., 2010)). Despite its importance, the VOS visually estimated weather reports are challenging for the derivation of precipitation intensities and are prone to large errors (Kent et al., 2010). Weller et al. (2008) gives an overview on existing types of gauges used over the ocean.

Optical rain gauges have been developed that record precipitation due to the blockage of a light or laser beam, but they are not readily calibrated by the user and are hence used with some reluctance (Weller et al., 2008). Occasional attempts have been made to install shipborne scanning and vertical pointing radars on research vessels (R/V) to measure precipitation, but the operation turned out to be difficult. Because of the inherent problems with conventional gauges, considerable effort went into developing hotplate precipitation sensors and distribution droplet meters (disdrometers) using acoustical, electro-mechanical, imaging and optical methods. A comprehensive overview on existing instruments and measurement principles is provided by Michaelides (2008). One of the biggest advantages of optical disdrometers over conventional gauges is measuring the precipitation rate through particle size distributions (PSDs), which, in case of rainfall is commonly referred to as the drop size distribution (DSD). PSDs are of great importance for understanding the microphysical processes governing the formation of precipitation, e.g. coalescence and ice-phase nucleation, breakup of large droplets into numerous small ones, evaporation of falling droplets, size sorting of particles in convective drafts, or wind shear effects. They are commonly used to validate the empirical relationship between radar-reflectivity and precipitation rate (Z–R relations), and to estimate the atmospheric attenuation of electromagnetic radiation caused by hydrometeors in the passive microwave spectrum (Rosenfeld and Ulbrich, 2003; Bringi and Chandrasekar, 2001). Cloud model calibration and consequently satellite-based precipitation retrieval algorithms benefit from the knowledge of averaged PSDs, distinct for precipitation phase, e.g., for different climatological regions (Tokay et al., 2001). Furthermore, PSD information is a crucial parameter for ground-based and spaceborne radars as well as passive microwave radiometers onboard satellites.

Taylor (2000) notes that optical disdrometers are regarded as the reference instrument for surface precipitation measurement. Post et al. (1998) emphasize the importance of disdrometer calibration for the reliable use of quantitative precipitation data. Optical disdrometers measure the light extinction by hydrometeors falling through a sensitive volume and overviews are provided by Illingworth and Stevens (1987), Bradley et al. (2000) and Frasson et al. (2011) among others.

Shipboard requirements for optical disdrometer operation under all-weather situations include reliable measurements at high wind speeds, frequently varying relative wind directions, flow distortion around the ships superstructure, ship movement in high sea states, and frozen precipitation. The limited knowledge about PSD over remote ocean areas in different climatic regimes and seasons is mainly due to the lack of suitable in-situ instrumentation and hence the absence of systematic data collection (Klepp et al., 2010; Bumke and Seltmann, 2011). In principle, gauges are usually inapplicable for this task, as they are prone to large errors, up to 100%, due to wind-induced undercatch and the inability to measure solid precipitation (Peterson et al., 1998). For rainfall measurements only, the specially designed ship rain gauge (Hasse et al., 1998) is also capable of providing reliable data on moving ships even under higher wind speeds. Simultaneous measurements of this ship rain gauge and the optical disdrometer ODM470 on the R/V Alkor over the Baltic Sea agree within 2% of accumulated rain, the correlation coefficient is 0.9, based on 1-minute measurement intervals (Bumke and Seltmann, 2011).

Recommendations of the International Precipitation Working Group (IPWG; Huffman and Klepp, 2011), GPM-GV (Hou et al., 2014), SeaFlux (Curry et al., 2004) and OceanObs (Fairall et al., 2010) communities are summarizing this surface reference measurement deficiency in expressing the urgent need for improved and innovative robust automatic sensors. These are required to allow the capability of providing high quality shipboard precipitation measurements over remote oceans for validation of satellite products and retrieval constraints. Precise information about the precipitation phase, intensity and PSD under all-weather conditions with appropriate statistical sampling is required. All satellite remote sensing precipitation products, re-analysis and models involving the air–sea system would benefit from increased shipboard sampling density and improved accuracy of precipitation measurements (Weller et al., 2008).

These needs motivated initiating OceanRAIN (Ocean Rainfall And Ice-phase precipitation measurement Network) at CliSAP/CEN, University of Hamburg and the Max Planck Institute for Meteorology in Hamburg, Germany in 2009, for high quality oceanic shipboard precipitation measurement in order to provide surface validation data. The present paper describes the instrumentation, the measurement procedure, operation, logistics and data set generation. OceanRAIN aims at a systematic shipboard data collection effort to establish a comprehensive statistical basis of phase-distinctive, temporally continuous records of precipitation (occurrence, intensity, accumulation, phase, PSD and ancillary meteorological data) in minute resolution for surface validation of satellite, re-analysis and model data. The OceanRAIN instrumentation, using the optical disdrometer ODM470, is the mainstay of the in-situ precipitation measurement, and was especially designed to perform under rough sea states and high wind speed conditions onboard moving ships in all-weather situations. Its advantages over other optical disdrometers are:

- The instrument's sensitive volume is pivoting around a vertical axis, keeping the sensitive volume always perpendicular to the local wind direction by aid of a wind vane.
- The cylindrical form of the sensitive volume causes the measurement to be independent of the incident angle of the hydrometeors so that local up- and downdrafts are not influencing the measurements.
- The optical unit allows discriminating 128 size bins resulting in a wide dynamic range of the PSD.
- The availability of a rain- and snowfall algorithm.
- The system is fully automatic and requires minimal maintenance.

To minimize the influence of sea spray and wave water, the ODM470's are mounted at heights between 30 and 45 m according to Reed and Elliot (1977). The selected ships operate since 2010 with long-term deployments in climate-relevant remote ocean areas (e.g. cold and warm season Arctic/Antarctic, Southern Oceans, subtropics, ITCZ, mid-latitude stormtracks). The research vessels do not circumvent high impact weather, resulting in a dataset including extreme values with rainfall up to 160 mm/h. Taylor (2000) estimates the number of in-situ precipitation measurements over the global ocean being no more than several thousand samples. By October 2014 the OceanRAIN collected already more than 370,000 high quality minute spectra, and thus can already be regarded as a major improvement for the science community. Precipitation occurs at approximately 10% of the time. The true-zero values recorded also carry important information for validation of false alarm statistics.

OceanRAIN provides increasing knowledge about oceanic precipitation, improving the error characterization of the GPM era satellite retrievals, which adds to the continual improvement of the satellite retrieval algorithms and to benchmarks of existing satellite, reanalysis and model climatologies. The data products (occurrences, intensities, accumulations, time series and PSDs) can be exploited statistically for specific oceanic areas, used for detailed process studies or to investigate the point-to-area problem when comparing point ship data to areal satellite estimates.

Section 2 provides a technical overview on the measurement principles of the OceanRAIN disdrometers and the data retrieval algorithms. The calibration procedures are described in Section 3. Section 4 introduces the data ingest, dataset production, and quality control procedures. Measurement examples are provided in Section 5. In Section 6, conclusions are provided with an outlook on the application potential of OceanRAIN for surface validation of remote sensing and modeling products.

2. The OceanRAIN instrumentation

2.1. ODM470 development

Originally developed at GEOMAR Kiel, Germany (Großklaus, 1996) with the purpose of ship rain gauge calibration, the ODM470-100 was built for rainfall measurements only and showed good performance regarding PSDs and rain rates (Clemens, 2002). The instrument was especially designed to perform with high accuracy under calm as well as high wind speeds, rough sea states, and irregular flow patterns onboard moving ships. The ODM470-200 was further developed and reconstructed to also measure the snowfall rate in having a logarithmic instead of linear size binning of the measured particles (Großklaus et al., 1998; Bumke et al., 2004). The instrument was operated on R/V "Knorr" over the cold-season Labrador Sea (Marshall et al., 1998). Lempio et al. (2007) implemented an additional snowfall algorithm and tested the disdrometer during an intercomparison field campaign in Uppsala, Sweden in winter 1999/2000. Results showed plausible higher values of the disdrometer at high wind speeds probably as a consequence of undercatch by the gauges. When cases with snowflakes larger than 9 mm in diameter are excluded from the analysis (due to retrieval limitations) 56 events showed a correlation coefficient of $r = 0.794$.

The optical disdrometer ODM470-200 demonstrated its potential in measuring liquid and solid precipitation over the cold-season Nordic Seas offshore of Norway during the campaigns LOFZY 2005 (Lofoten Cyclones; Klepp et al., 2010; Brümmer et al., 2010), onboard R/V 'Celtic Explorer', and THORPEX IPY 2008 (International Polar Year), onboard the Norwegian Coast Guard ship K/V 'Senja'. For monitoring and quality control of the disdrometer data, the precipitation detector IRSS88 (see Section 2.2) was operated independently, accompanied by a detailed observer's precipitation log. The dichotomous verification of the precipitation frequency between the ODM470-200, the detector and the observer's log resulted in a perfect score, giving confidence in the collected disdrometer surface validation data (Klepp et al., 2010). The HOAPS (Hamburg Ocean Atmosphere parameters and Fluxes from Satellite Data; Andersson et al., 2010) precipitation was overall consistent with the ODM470-200 snowfall data, with a detection accuracy of 96%, a bias score of 94%, a hit rate of 90%, a false alarm ratio of only 4% and a probability of false detection of only 2% (Klepp et al., 2010). The ship-to-satellite collocation utilized a 55 km radius around the ship position with a temporal criterion of ± 45 min centered on the overflight time of the satellite. In contrast, GPCP 1DD (Global Precipitation Climatology Project 1 Degree Daily; Huffman and Co-authors, 1997) and GPROF2004 (Goddard Profiling Algorithm Version 2004; Kummerow et al., 2001) data turned out to be not sensitive to solid precipitation at high-latitudes (Klepp et al., 2010). However, during these campaigns, only light snowfall events up to 1 mm/h fell into the strict collocation criteria for the satellite overpasses of the HOAPS climatology. Nonetheless, when accepting larger spatio-temporal collocation mismatches, data of intense snowfall comparisons up to 7 mm/h between the ODM470-200 and HOAPS data also yield plausible results (Brümmer et al., 2010).

Alongside the international science request for high quality surface validation data of precipitation over the oceans, as outlined in the introduction, the encouraging results of these field campaigns motivated initiating OceanRAIN in 2009. For this purpose the disdrometer was further developed into an automated computerized data logging measurement system and is now commercially available by the company Eigenbrodt GmbH & Co. KG, located in Königsmoor near Hamburg, Germany.

2.2. The OceanRAIN automated measurement system

The ODM470-100, with linear size binning for rainfall measurements only, and the ODM470-200, with logarithmic size binning (Section 2.3) and changed electronics for rain and snowfall measurements were prototype instruments. These versions required surveillance and onboard personnel when operated onboard ships. Experience with their operation during the cold-season cruises in the Nordic Seas (LOFZY and THORPEX; Section 2.1) led to a number of improvements for routine operation.

For the long-term deployment purposes of OceanRAIN, it became finally necessary to use this experience to automate the instruments for autonomous and reliable operation under all-weather situations. The first automated maintenance-free version was the ODM470-300, of which three newly built instruments were successfully operated onboard ships between 2010 and 2012. The disdrometer design was subsequently changed to further reduce flow distortion caused by the instrument itself. The wind vane was reconstructed to be more robust. The disdrometer electronics were updated to communicate with recent computer systems. In total, three cables of the disdrometer, detector and anemometer (Fig. 1) run from the ships mast down through a water proof gasket into a dry lab, where they were connected to an interface box that was attached to a PC.

The interface box received an additional port for the opto-electronically infrared rain sensor (IRSS88) that measures the

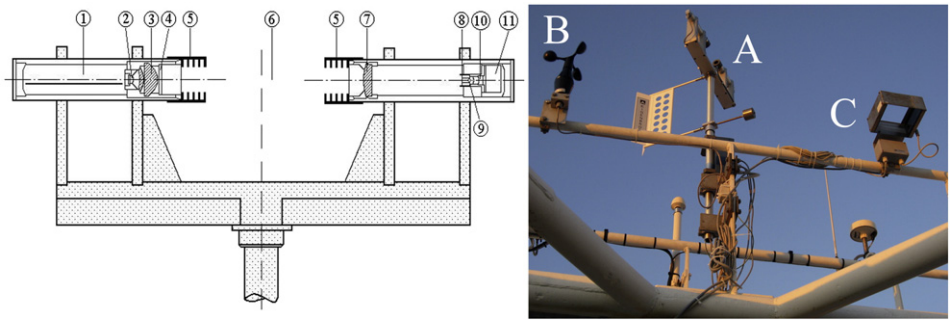

Fig. 1. Cross-section of the optical disdrometer ODM 470. From left to right: electronics (1), light emitting diode (2), lens system (3), window (4), baffles (5), sensitive volume (6), achromatic collector lens (7), optical blend (8), ocular (9), photo diode (10), electronics compartment (11). The image shows the setup of the ODM470-300 automatic measurement system with the disdrometer (A), the anemometer (B) and the precipitation detector IRSS88 (C) in the highest parts of the mast onboard R/V 'Polarstern'.

precipitation occurrence. The instrument houses two high-intensity infrared beams generating an active sensing area of about 120 mm by 25 mm. The system is able to detect small-sized hydrometeors that pass through the sensing area. The sensor is mainly used to switch-off the disdrometer 1 min after the last precipitation occurrence. Eight particles crossing the sensing area of the IRSS88 are needed to switch the disdrometer on again. This mutual connection has many advantages. Evaluation of the data shows that precipitation over the oceans occurs approximately 10% of the time. It is therefore necessary to prolong the lifetime of the diodes by switching off the disdrometer during no precipitation. Furthermore, artificial signals produced by vibration during no precipitation periods are no longer recorded, as the IRSS88 prevents switching on the disdrometer. Additionally, artifacts crossing the sensitive volume of the ODM470 are no longer erroneously recorded as precipitation signals (Section 2.6).

The almost maintenance-free system uses an automatic data backup written to the internal hard drive and to a memory stick. The PC is plugged into an Uninterruptible Power Supply (UPS) that buffers power outages up to 45 min. Experience showed that short power outages on ships may frequently occur, making such precaution measures important. In case of an unexpected system shutdown, the PC reboots automatically and the data logging software restarts without personal assistance. The ODM470-300 setup was successfully tested to not interfere with other shipboard equipment.

The experience gained with the ODM470-300 version led to further improvements that were implemented during 2012. With the most recent version, the ODM470-400, which is in operation on all ships since late 2012, the system software is changed to Linux and the former combination of an interface box and a data logging PC is replaced by an embedded PC including a data display. The data is stored to a solid state disk and a SD card. The formerly three individual cables are combined into a single one. The cup anemometer is exchanged with a more robust version, including a metal housing and a redesigned seawater-proof cable plug. The software is updated to store not only the minute data records but also the raw data of each particle during the integration time of 1 min, also, the data format was updated. Days without precipitation occurrence are now also logged with empty files including the header only to assure that the instrument was correctly working. Section 2.3 describes the electronic procedure of particle size detection using the comparator. The signal is transmitted via a high- and low-pass filter to a peak detector. This method was developed for the ODM470-200 version snowfall disdrometer and is also applicable for rainfall. Nonetheless, the initial rainfall disdrometer of version ODM470-100 amplified this signal by a factor of 13 to exclude errors resulting from unrealistically large drops (>6.4 mm in diameter). Additionally, the ODM470-100 version had a different time constant for the flip-flop that terminates the residence time count of a particle to prevent implausible fall velocities. The ODM470-400 version combines the advantages of the rain- and snowfall measurements in storing the data of both methods separately within the raw data files. Once the precipitation phase is identified (Section 4.3), either the rain or snowfall spectra are used to calculate the precipitation rates. All three ODM470-300 systems were upgraded to ODM470-400 standard and three new ODM470-400 versions were additionally acquired for OceanRAIN.

The representativeness and conformity of measurements between the instrument versions are guaranteed by the calibration procedure that is described in Section 3. In the following, the disdrometer system is described in detail.

2.3. Measurement principles and technical realization

The mainstay of the OceanRAIN setup is the optical disdrometer ODM470 (Fig. 1). The measurement principle is based on light extinction caused by hydrometeors passing through a cylindrical sensitive volume of 120 mm length and 22 mm diameter. This volume is homogeneously illuminated by an infrared light emitting diode at 880 nm wavelength on one side of the volume. A photo diode receiver is placed on the other side. Collector lenses and an optical blend assure for homogeneity and isotropy of the light in the volume. A detailed technical description of the optical system is provided by Lempio (2006). The instrument is pivoting around a vertical axis by aid of a wind vane, keeping the sensitive volume always perpendicular to the local wind direction. The cylindrical form of the volume causes the measurement to be independent of the incident angle of the hydrometeors so that local up- and downdrafts are not influencing the measurements (Lempio et al., 2007).

While there is no particle in the sensitive volume, the instrument measures a reference voltage of about 5 V. Particles cause this voltage to decrease with increasing light attenuation down to an activation voltage. Complete blockage of the sensitive volume may lower the activation voltage to 0 V corresponding to a particle of 22 mm in diameter. A comparator measures the difference in voltage that is proportional to the size of the particle. Hence, the light intensity at the receiver decreases with increasing particle size, causing the electronic signal of the hydrometeor to be proportional to its cross-sectional area. During the integration time of 60 s, all hydrometeors falling through the sensitive volume are counted and partitioned according to their cross-sectional area into 128 size bins (D_p = particle diameter), with a wide dynamic range from 0.01 to 22.28 mm (Fig. 2; Table 1) and a logarithmic increasing particle diameter to improve resolution at smaller particle sizes (Eq. (1)). Accordingly, the bin width ranges from 0.04 mm at bin 14 to 0.56 mm at bin 128.

$$D_p(\mathrm{bin}) = \frac{e^{\left(\frac{\mathrm{bin}}{94}\ln 10\right)} - 1 + e^{\left(\frac{\mathrm{bin}+1}{94}\ln 10\right)} - 1}{2} \quad [\mathrm{mm}] \tag{1}$$

Additionally, the residence time of the particles in the sensitive volume, which depends on the fall velocity of the particles and the wind speed is stored. Due to the moving ship, the latter is measured as a relative wind speed using the cup anemometer (Fig. 1) with an averaging

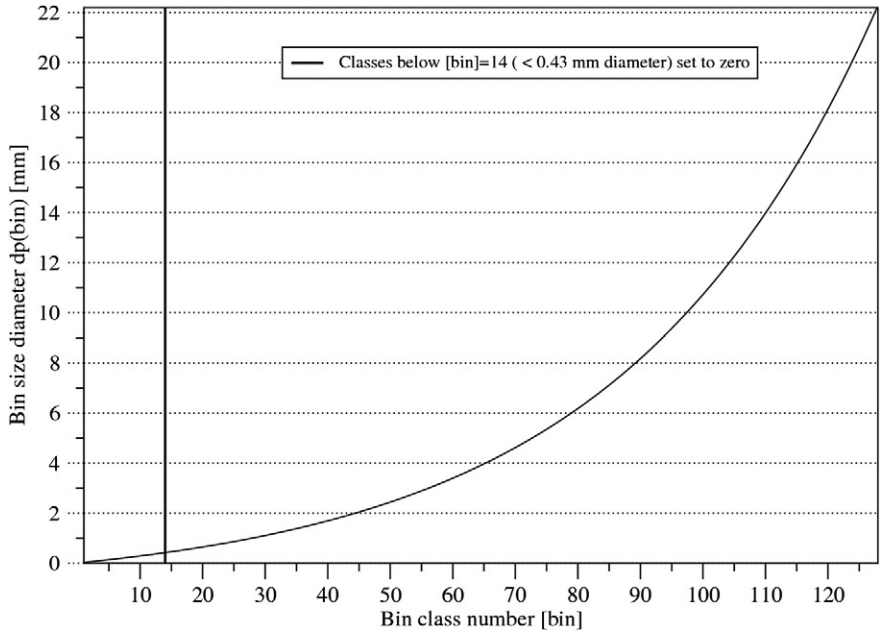

Fig. 2. Bin size diameter versus bin class number of 128 size bins after Eq. (1).

time period of 1 min as part of the measurement setup. If the residence time of a particle exceeds an unrealistically high value, the measurement is terminated and considered an artifact and is thus discarded, e.g., an artificial blockage of the sensor or a lump of sliding snow. Vibration of the disdrometer due to gusty winds or ship propulsion influence transferred to the disdrometer mounting may cause temporary loss of adjustment of the instruments optics. In turn, this may cause artificial signals within size bins smaller $D_p = 0.3$ mm. Such artifacts cannot be separated from real precipitation signals. Hence, data below size bin 14 (<0.43 mm) are excluded from the analysis. However, the contribution of these small size bins to the precipitation rate (under non-vibrating conditions) is insignificant (not shown) and only affect the PSD starting at particle sizes >0.43 mm in diameter.

Table 1
128 bins with corresponding bin size D_p (bin) center in mm after Eq. (1).

bin	D_p (bin)	bin	D_p (bin)	bin	D_p (bin)	bin	D_p (bin)	bin	D_p (bin)
001	0.04	027	0.96	053	2.71	079	6.01	105	12.26
002	0.06	028	1.01	054	2.80	080	6.19	106	12.58
003	0.09	029	1.06	055	2.90	081	6.36	107	12.92
004	0.12	030	1.11	056	2.99	082	6.55	108	13.27
005	0.14	031	1.16	057	3.09	083	6.73	109	13.62
006	0.17	032	1.22	058	3.19	084	6.92	110	13.98
007	0.20	033	1.27	059	3.30	085	7.12	111	14.35
008	0.23	034	1.33	060	3.40	086	7.32	112	14.73
009	0.26	035	1.39	061	3.51	087	7.53	113	15.12
010	0.29	036	1.45	062	3.62	088	7.74	114	15.52
011	0.33	037	1.51	063	3.74	089	7.96	115	15.93
012	0.36	038	1.57	064	3.86	090	8.18	116	16.35
013	0.39	039	1.63	065	3.98	091	8.41	117	16.78
014	0.43	040	1.70	066	4.10	092	8.64	118	17.23
015	0.46	041	1.76	067	4.23	093	8.88	119	17.68
016	0.50	042	1.83	068	4.40	094	9.12	120	18.14
017	0.54	043	1.90	069	4.49	095	9.38	121	18.62
018	0.57	044	1.98	070	4.62	096	9.63	122	19.10
019	0.61	045	2.05	071	4.76	097	9.90	123	19.60
020	0.65	046	2.12	072	4.91	098	10.17	124	20.11
021	0.69	047	2.20	073	5.05	099	10.44	125	20.63
022	0.74	048	2.28	074	5.20	100	10.73	126	21.17
023	0.78	049	2.36	075	5.36	101	11.02	127	21.72
024	0.82	050	2.45	076	5.51	102	11.32	128	22.28
025	0.87	051	2.53	077	5.68	103	11.62		
026	0.91	052	2.62	078	5.84	104	11.93		

The minute resolution data record headers contain the date, time in UT (Universal Time coordinate), reference voltage, relative wind speed, number of allocated bins with at least one particle, accumulated number of particles in these bins, and the integrated residence time for every bin. As only minutes with precipitation occurrence (at least 8 particles per minute) are recorded, the time series produced by the disdrometer is discontinuous. The data is written into daily files that are empty if no precipitation occurred. This allows controlling that the data logging system is correctly working without interruptions.

2.4. Particle size distributions

The PSD density $n(\text{bin})$ in $[1/\text{m}^3]$ is calculated after Clemens (2002) from the recorded particle number per size bin $N(\text{bin})$ and the relative wind speed U_{rel} measured by the cup anemometer. The sensitive volume has a length of $l = 120$ mm with a diameter $d = 22$ mm. This results in a cross-sectional area of 26.4 cm^2 and a corresponding sensitive volume of 45.6 cm^3. The measurement interval is set to $t = 60$ s. Together with the geometrical sum of the relative wind speed and the parameterized terminal fall velocity V_{fall} (Eqs. (3) and (4)), the PSD density is given by Eq. (2):

$$n(\text{bin}) = \frac{N(\text{bin})}{l \cdot d \cdot t \cdot \sqrt{{U_{rel}}^2 + (V_{\text{fall}}(\text{bin}))^2}} \quad \left[\frac{1}{\text{m}^3}\right] \tag{2}$$

The PSD density can in principle also be derived using the recorded residence time. However, the residence times of particles of the same size can vary depending on the path flown (margin, center or along-drift) through the sensitive volume. Thus, Clemens (2002) and Lempio et al. (2007) showed that the particle counting method (Eq. (2)), used to derive the PSD density, leads to improved results over the residence time method when the relative wind speed is additionally measured. Consequently, the geometric effect of the residence time no longer affects the measurement, as the PSD density $n(\text{bin})$ is calculated using a pre-defined volume under the assumption of a uniform distribution of the hydrometeors (Lempio, 2006).

To determine the number concentration $\left[\frac{1}{\text{m}^3}\frac{1}{\text{mm}}\right]$, the lower and upper bound of $D_p(\text{bin})$ is calculated after Eq. (1) to normalize the PSD $n(\text{bin})$ with the non-constant bin interval width. This leads to the

minute spectra of number concentrations. During 1 min of precipitation, usually not all 128 size bins are allocated with values and hence are allocated with zero values in the PSD data. When averaging the minute-based number concentrations over a given time period and/or area, the sum of the number concentration per bin is divided by the total number of spectra (number of minutes). It is important to note that the spectra divisor (e.g. 30,000 selected spectra of snowfall) is constant throughout the 128 bins, as the small size bins are almost always allocated while large size bins are allocated infrequently and often contain zero values. Furthermore the total number of particles per size bin and minute is stored.

2.5. The rain and snowfall algorithm

The determination of the precipitation rate requires the liquid water content or mass of the particle $M_{\text{particle}}(\text{bin})$ and the terminal fall velocity $V_{\text{fall}}(\text{bin})$. These are parameterized after (Atlas and Ulbrich (1974); Eqs. (3) and (4)), as rain drops have a nearly spherical shape and a constant density.

$$M_{\text{particle}}(\text{bin}) = \frac{4}{3}\cdot\pi\cdot 1000\cdot\left(\frac{D_p(\text{bin})}{200}\right)^3 \quad [\text{kg}] \tag{3}$$

$$V_{\text{fall}}(\text{bin}) = 9.65 - 10.3\cdot e^{\left(-1.2\frac{D_p(\text{bin})\cdot 10}{2}\right)} \quad [\text{m/s}] \tag{4}$$

In contrast to rainfall, solid precipitation is characterized by a variety of complex shapes with different fall velocities and different equivalent liquid water content even if identical in the maximum dimension. The measured cross-sectional area depends on size, shape and orientation of the solid particles, hindering the development of a unique solid precipitation retrieval scheme. The relationship between mass or equivalent liquid water content and the terminal fall velocity for snow crystals is analyzed by Hogan (1994) as a function of their maximum dimension. However, the disdrometer measures the size of the cross-sectional area that depends on the orientation of the non-spherical particle instead of the maximum dimension. Assuming that the ice crystals fall randomly oriented through the sensitive volume (Brandes et al., 2007) and that a large sample of crystals of the same type has a repeatable mean cross-sectional area, the parameterization of Hogan (1994); Eqs. (5) and (6) can be used for the mass and terminal velocity of the snowflakes. This allows the derivation of a transformation function to estimate the maximum dimension of the crystal type from the mean cross-sectional area, and hence the equivalent liquid water content (mass) $M_{\text{particle}}(\text{bin})$ and terminal fall velocity $V_{\text{fall}}(\text{bin})$,

$$M_{\text{particle}}(\text{bin}) = 0.0000107\cdot\left(D_p(\text{bin})\right)^{3.1} \quad [\text{kg}] \tag{5}$$

$$V_{\text{fall}}(\text{bin}) = 7.33\cdot\left(D_p(\text{bin})\right)^{0.78} \quad [\text{m/s}] \tag{6}$$

However, the disdrometer cannot identify the type of a particle. Hence, Macke et al. (1998) developed a geometrical model to simulate different snow crystal types and a ray tracing model to determine the mean cross-sectional area out of 3000 randomly oriented projections for different sizes with regard to their maximum dimension. Lempio et al. (2007) found that the product of the terminal velocity and the equivalent liquid water content as a function of the cross-sectional area of different types of snow crystals are of the same order of magnitude, and allows using one common parameterization for lump graupel. As lump graupel is nearly spherical in shape, it needs no transformation function from cross-sectional area to maximum dimension. The parameterization for lump graupel underlying the snowfall algorithm is applicable for particles with a size range of 0.43 to 9 mm. Consequently, solid precipitation consisting of large snowflakes results in less certain precipitation rates. However, PSD results from Section 4.5 (Fig. 8) will show that the absolute number of measured snowflakes already drops below 600 (and 350 snowflakes in the mixed-phase PSD) at size bin 94 ($D_p > 9$ mm). This infrequent occurrence of large particles demonstrates that the associated error on the total precipitation is negligible. In contrast, lump graupel below 9 mm in size was the most frequently observed precipitation type over the Nordic Seas during the LOFZY campaign (Klepp et al., 2010). To date, no mixed-phase precipitation algorithm is available and the snowfall algorithm is applied for these cases. The assignment for mixed-phase precipitation is performed using ancillary data and the resulting uncertainties are discussed in Section 4.4.

In either case of rain or snow (liquid water equivalent), the precipitation rate P in [kg/m^{2}h] or [mm/h], respectively, is calculated by multiplying the constant 3600 to account for the hour unit with the product of the PSD density, the terminal fall velocity for rain (or snow), and the mass of the rain droplet (or liquid water equivalent of the solid particle). In analogy to the rainfall estimation by Pruppacher and Klett (1978), the following expression was derived by Großklaus (1996) for the precipitation rate.

$$P = 3600\cdot\sum_{\text{bin}=0}^{128} n(\text{bin})\cdot V_{\text{fall}}(\text{bin})\cdot M_{\text{particle}}(\text{bin}) \quad [\text{mm/h}] \tag{7}$$

2.6. Error source handling

Sampling of precipitation using a three-dimensional sensitive volume is by definition prone to error sources, such as edge effects of partly scanned hydrometeors, coincidence effects of multiple hydrometeors within the sensitive volume at the same time, artificial hydrometeors produced from impacting the instrument housing, riming, or collection of snow on the hoods that slide into the volume under low wind speed conditions. Additionally, artificial hydrometeors may be produced by insects, pollen and spider webs although these error sources are fairly infrequent onboard ships.

Edge effects occur when parts of a particle are located outside of the sensitive volume and are only registered if the center of the particle is within the volume. The resulting particle appears smaller and would result in a lower terminal fall velocity and lower mass. Hence, such hydrometeors tend to underestimate the precipitation, as they are stored in size bins which are too small. In contrast, coincidence effects of overlapping hydrometeors within the volume lead to enlarged particles and hence would overestimate the precipitation contribution and are prone to false placement in size bins which are too large. Both effects interact, and their statistical correction procedures have been discussed in detail for rainfall by Großklaus (1996) and Lempio (2006) using actual minute measurements to estimate the probability of edge and coincident effect occurrences and their shift and split in bin size.

Effects of artificially small particles due to splashes of impacting raindrops on the housing of the instrument or snow accumulation in or on the hoods are minimized by the design of the disdrometer. The base metal plate has a triangular shape that deflects splashing droplets away from the sensitive volume and is also not prone to collect snow as it will slide sideways. Ice rain, riming or swirling snow in low wind conditions are considered problematic and data of such events is excluded from the analysis. To prevent wet lenses from affecting the measurements, a special filtering is implemented that excludes signals exceeding a threshold of the residence time.

Finally, spider webs are not a frequent problem on moving ships. Still the data can be inspected for such recurring patterns and are considered by the software during the calculation of the PSD and precipitation rate. Recordings of insects or pollen are avoided using a coupled precipitation detector IRSS88. Even if insects or pollen would cross the sensitive volume they would still not be recorded unless precipitation

is present. The purpose of the IRSS88 as part of the automated measurement system is described in Section 2.2.

3. The OceanRAIN instrument calibration

A prerequisite to ensure high quality PSD measurements and rates of liquid and solid precipitation is a rigorous calibration of each disdrometer. Calibration follows a two-step approach of electronic hardware calibration in the laboratory followed by test site calibration using real precipitation events. This procedure is performed in close cooperation with the manufacturer Eigenbrodt. The calibration steps are described in the following and apply to new instruments as well as instrument maintenance after shipboard usage.

3.1. Hardware calibration

As a first calibration step, the optical axis within the sensitive photoelectric volume is calibrated to homogeneously illuminate the cylindrical volume with a constant diameter of 22 mm. To achieve this, the optical axis of the diode can be tilted. A rotating wire is brought into the sensitive volume and an oscilloscope is connected to the main board of the disdrometer electronics. Correctly calibrated, the oscilloscope shows a semi-circle of the optical attenuation with time, or bulging distortion otherwise. This is repeatedly done along the optical volume length of 120 mm. Additionally, the reference voltage is adjusted to 5.2 V using a potentiometer of the receiver side of disdrometer.

The ensuing laboratory calibration focuses on adjustments of six potentiometers in the opto-electronic emitter/receiver device and the electronic main board of the ODM470. Two potentiometers control the analog-digital transformer and the offset of the operation-amplifier for 0 V. The remaining two potentiometers are of special importance. They control the size and detection sensitivity of a metal reference sphere of 0.5 mm diameter which is dropped through the optical volume of the disdrometer. Once the potentiometer adjustment measures the correct size value of the spherical, it is crucial that the other potentiometer is logging the right amount of 0.5 mm spheres. Tuning of this potentiometer to its extreme values either results in zero-detection of spheres or an infinite number of spherical artifacts. This is essential, as strong vibration of the light barrier in the optical system causes small artificial drops (Section 2.3). Vibration of the instrument is an important issue onboard ships, as all mast or railing parts where the instrument is mounted are prone to vibration that either results from the ship engine, sea state, or ice-breaking activity. A correct calibration of this potentiometer allows for the detection of all dropped 0.5 mm reference spheres while suppressing all artificial drops due to vibration. Experience onboard ships show that this procedure works with high precision, as during precipitation-free periods, no artificial drops are recorded by the disdrometer. As a next step, a reference spherical of 6.0 mm diameter is used to derive the disdrometer constant. This amplification value controls the precipitation volume recorded. Increasing the disdrometer constant leads to smaller drops and hence less volume of precipitation. Finally, ten test spheres of increasing size (0.5, 0.8, 1.5, 2.5, 3.5, 4.0, 6.0, 10.0, 12.0 and 16.0 mm diameter) are repeatedly dropped through the sensitive volume. If the measured diameter range deviates from the input spherical diameters, the calibration procedure is repeated from the beginning.

3.2. Rainfall verification

After successful hardware calibration the instruments are mounted outside on a test field for performance tests with real precipitation events. The minute precipitation rates and accumulations of the disdrometer are compared to those from a reference automatic weighing gauge ANS410. This instrument is also built by Eigenbrodt and measures liquid and solid precipitation using a Hellmann WMO standard 200 cm^2 collector area, a precision pressure sensor to determine the precipitation amount and intensity, a collector shape that reduces the undercatch due to wind effects, and a heating system for solid precipitation. The ANS410 was successfully tested among 30 other rain gauges during a field campaign carried out by the WMO in 2007 in Italy (Lanza and Vuerich, 2009). For intercomparison purposes, the ANS410 is used in a 0.6 mm/h step-weighing configuration, and precipitation data is used only if the relative wind speed is below 5 m/s to avoid gauge undercatch to the maximum extent possible. Bumke and Seltmann (2011) showed that the deviations between a Hellman rain gauge and a ship rain gauge of a five year time record is less than 2% for wind speeds below 5 m/s. For higher wind speeds, during an extreme precipitation event of about 280 mm precipitation accumulation within two days and snowfall periods, the OceanRAIN disdrometer showed reliable performance. Results are expected from the WMO (World Meteorological Organization) field experiment SPICE (Solid Precipitation Intercomparison Camgaign;http://www.wmo.int/pages/prog/www/IMOP/intercomparisons/SPICE/SPICE.htm) and are in preparation for publication. Due to the different measurement principles of both instruments (PSD versus discrete weighing gauge steps per minute), neither minute resolution correlations nor scatter diagrams of the values are presented here. The rainfall time series of both instruments are used to aggregate the data to hourly sums over the precipitation event. The minimum time for intercomparison is three hours to assure a statistical basis of at least 180 min of data. The total amount of precipitation is used to estimate the bias in terms of percentage deviation between both instruments. As rain drops can stick to the side walls (wetting losses) of the ANS410 that may evaporate before reaching the collector, it is expected that the ODM470 will slightly outperform the values of the ANS410 for rainfall at low wind speeds.

Fig. 3 shows the time series of a typical calibration event for the ODM470-400 at the test site at Eigenbrodt company near Hamburg, Germany. On 31 May 2012 from 16 to 23 UT, Central Europe was affected by an intense summertime cyclone at a temperature of 12 °C. Northern Germany was located beneath the warm front during the first hour with drizzle below 2 mm/h. From 17 to 21 UT, rain fell with changing intensities from the occlusion area of the cycle head, with individual showers of up to 22 mm/h. Around 22:30 the northern branch of the cold front led to intense showers of up to 19 mm/h. For the last hour the precipitation rate steeply dropped below 1 mm/h and ended at 23 UT. The overall shape of the rainfall time series is well represented by both instruments, and the data agrees well for the low and high rain rates of the different frontal structures (Fig. 3a and b). The expected delay effect of the ANS410 data is visible when zooming into both time series (Fig. 3c) as the ODM470 records the real number of drops in each class per minute while the ANS410 measures per minute in discrete intervals when 0.6 mm is reached. This leads to the effect that the red bars are often visible with a shift of a minute to the right of the black ODM470 bars. This is the main reason why aggregated hourly values and total accumulation is compared in the following instead of individual minute values.

The minute data in mm/h of both time series is divided by 60, integrated to hourly sums and aggregated to the total amount of precipitation during the cyclone passage. The blue bars in Fig. 4 show hourly rainfall accumulations of the ODM470, while the blue line is the total accumulation over time. Values in red represent the ANS410 data, respectively. The hourly bars of both instruments are in good agreement and the accumulation curves are almost on top of each other. The cyclone accumulated a total of about 20 mm of rainfall in 8 h. The ODM470 indicates about 0.26 mm more precipitation compared to the ANS410, corresponding to an excess of 1.3%.

If the deviation between both instruments is better than 2%, the calibration is considered successful and the ODM470 instrument is ready for shipboard operation. Readjustments of the hardware components and a new calibration are necessary if the deviation is repeatedly larger than 2%. Instruments returned from shipboard operation are

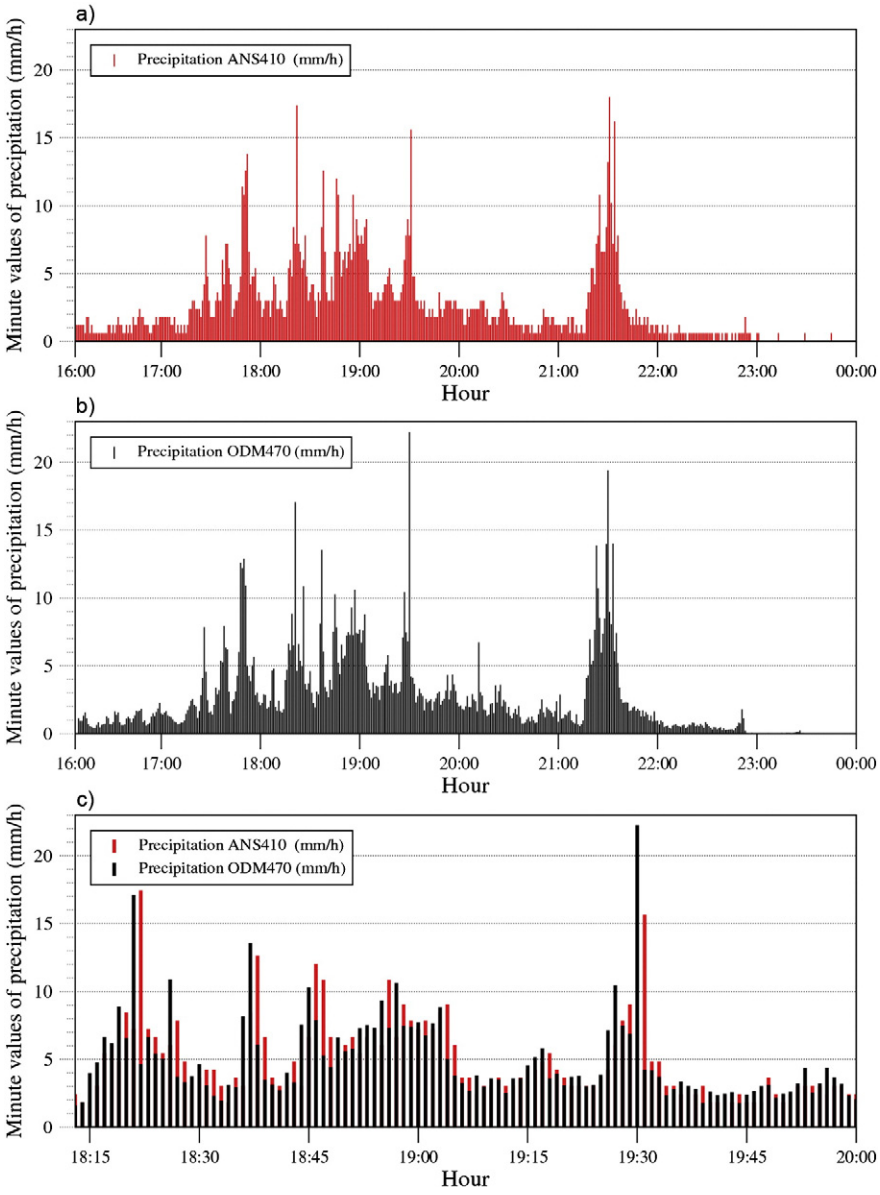

Fig. 3. Time series of precipitation calibration test between the ANS410 (a) and the ODM470 (b) in mm/h min values during the passage of a cyclone on 31 May 2012 between 16 and 23 UT over Northern Germany. The lower panel (c) illustrates a zoom into the time series to demonstrate the temporal lag of the ANS410 (red) over the ODM470 (black) as a consequence of the gauge measurement technique.

investigated for calibration drift during the measurements compared to its initial state to ensure homogeneous data quality.

4. OceanRAIN methodology

The long-term data acquisition within OceanRAIN aims at systematic data collection, quality controlling, archiving, analyzing, and the distribution of high quality shipboard surface precipitation data by providing flag separations for the precipitation phase, through applying rain- and snowfall algorithms for occurrence, intensities, and accumulations together with phase-distinctive PSDs in minute intervals. The scope of the data collection effort also comprises the collection of ancillary automated surface meteorological data and navigational data provided by the ship operators together with ship bridge weather and precipitation type observations. These separately recorded incoming data streams are navigated, collocated, quality controlled, and checked for metadata and data reliability, and are finally merged into the OceanRAIN data products. These products contain precipitation intensity time series and PSDs in minute intervals and are analyzed and distributed with the goal of providing a comprehensive statistical basis of global ocean precipitation for all climatic regions. Suspect and erroneous data are rigorously excluded from the data records using automatic preprocessing routines followed by visual inspection of all parameters and metadata checks. The output is written to standard ASCII and netCDF format. In the following, the procedures of the data set construction are described in detail.

4.1. Shipboard operation

A comprehensive overview on the shipboard measurement activities in chronological order is given in Table 2. The roots of the OceanRAIN data collection date back to the snowfall measurement campaigns LOFZY and THORPEX in 2005 and 2008 over the cold-season Nordic Seas. The long-term routine measurements began in June 2010 onboard the German icebreaker R/V 'Polarstern' of Alfred Wegener Institute (AWI) and in September 2010 onboard the Russian R/V 'Akademik Ioffe' in cooperation with P.P. Shirshov Institute of Oceanology, RAS, Moscow. Both ships routinely transect the entire Atlantic

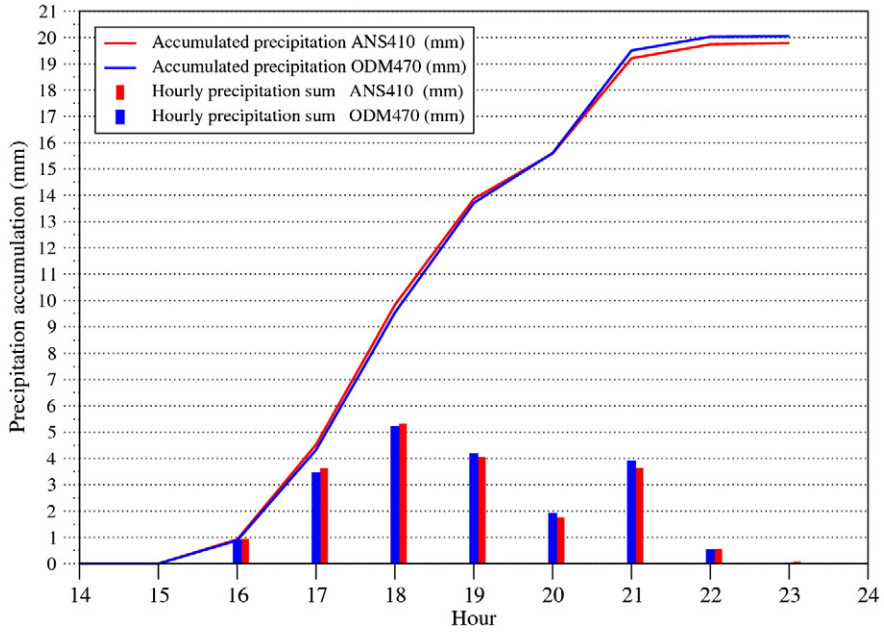

Fig. 4. Calibration test of hourly rainfall sums (bars) and total accumulated precipitation (curves) during the passage of the low pressure system of Fig. 3 in mm for the ODM470 in blue and the ANS 410 in red.

Ocean from the Inner Arctic through the mid-latitudes, the subtropics and the ITCZ to the Southern- and Antarctic Ocean, allowing for precipitation measurements in all climatic regimes. In September and October 2010, OceanRAIN took part in the LPVEX (Light Precipitation Validation Experiment) campaign embedded in GPM-GV in the Baltic Sea area off the coast of Helsinki onboard R/V 'Aranda' in cooperation with the Finnish Meteorological Institute (FMI). The aim of this campaign was to measure light precipitation from a variety of instruments, both on land and over the sea. Since December 2011, the German R/V 'Maria S. Merian', operated by Briese Research, is equipped, with a focus on subtropical, tropical and mid-latitude rainfall over the Atlantic Ocean. All three ships were re-equipped in September and October 2012 with the new ODM470-400 after 28 months of continuous measurements with half yearly maintenance intervals on R/V 'Polarstern', 25 months of continuous measurements with no maintenance possibilities onboard R/V 'Akademik Ioffe', and 9 months of continuous measurements onboard R/V 'Maria S. Merian'. The OceanRAIN disdrometer was additionally installed onboard the German R/V 'Sonne', owned by Partenreederei MS Sonne, during a cruise from Busan, South Korea to Fiji Islands in the Pacific Ocean in September and October 2012. Long-term measurements with a focus on the tropical Atlantic Ocean started in March 2014 onboard R/V 'Merian'. From November 2014 onward, a disdrometer will be mounted on the new German R/V 'Sonne' for long-term measurements in the Pacific and Indian Ocean. In 2015, a shipboard precipitation sensor intercomparison is planned onboard the South African R/V 'S.A. Agulhas II'. During the circum-Antartic cruise, a snowfall video imager, a Parsivel and an OceanRAIN disdrometer will be installed. An additional disdrometer is planned to be installed on the new Australian R/V 'Investigator' for data collection in the Pacific and Southern Oceans from 2015 on.

At present, four long-term and four short-term campaign-based deployments were made onboard a total of eight ships. All deployments have in common that data is collected over important remote ocean regions that are considered climate related hotspots. The measurement areas comprise both hemispheres including the sea-ice areas, the northern and southern mid-latitude stormtracks, the subtropics, and the ITCZ.

Table 2
Ship operation of all 7 ODM470 disdrometers.

ODM 470 #	Ship name or place of usage	Call sign	Start date	End date	Area of operation	ODM470 version remarks
1	R/V Celtic Explorer	EIGB	02/2005	03/2005	Nordic Seas	−200
	K/V Senja	LBHB	02/2008	03/2008	Nordic Seas	−200
	Hamburg, Germany		01/2009	11/2011	Lab Calibrator	discarded 11/2011
2	R/V Polarstern	DBLK	06/2010	10/2012	Atlantic Ocean	−300
	Hamburg, Germany		10/2012	10/2012		conversion update
	R/V Polarstern	DBLK	10/2012	ongoing	Atlantic Ocean	−400
3	R/V Akademik Ioffe	UAUN	09/2010	10/2012	Atlantic Ocean	−300
	Hamburg, Germany		10/2012	10/2012		conversion update
	R/V Akademik Ioffe	UAUN	10/2012	ongoing	Atlantic Ocean	−400
4	R/V Aranda	OHLV	09/2010	10/2010	Baltic Sea	LPVEX campaign
	R/V Maria S. Merian	DBBT	12/2011	09/2012	Atlantic Ocean	−300
	Hamburg, Germany		09/2012	09/2012		conversion update
	R/V Maria S. Merian	DBBT	09/2012	ongoing	Atlantic Ocean	−400
5	R/V Sonne	DFCG	09/2012	10/2012	Pacific Ocean	−400
	Boulder, USA	–	03/2013	04/2014	Snowfall Experiment	SPICE Project
	R/V Sonne (II)	DBBE	11/2014	long-term	Pacific/Indian Ocean	−400
6	R/V Meteor	DBBH	03/2014	ongoing	Altantic Ocean	−400
7	R/V S. A. Alguhas II	ZSNO	2015	12/2015	Antarctica	−400

Moreover, these ships do not circumvent high impact weather (e.g. storms) to avoid a bias in extreme conditions. To reduce airflow distortion and the effects of sea spray and wave water to a maximum extent possible, Bradley and Fairall (2007) suggest placement of the sensors in the highest parts of the ships mast, and, consequently, the disdrometers are installed between 30 and 45 m height. The deployment in the mast of R/V 'Polarstern' is shown as an example in Fig. 1 with the ODM470-300, the IRSS88 and the cup anemometer.

4.2. Shipboard data ingest

Four different shipboard data streams require merging and collocation to calculate navigated precipitation rates and PSDs categorized into liquid, solid and mixed-phase (Fig. 5). This comprises the ODM470 precipitation data (ODM) along with the ancillary shipboard navigation (NAV), meteorological and weather observation data (MET). The ODM data stores time, bin size, number of particles in each bin, residence time in the sensitive volume for both liquid and solid particles, plus relative wind speed and reference voltage in minute resolution. It is important to note that the precipitation phase is not identified by the instrument and that the ODM time series is discontinuous in the sense that only minutes containing precipitation are logged into daily files. Hence, data files of days without precipitation contain only the file header. Preliminary PSD and precipitation time series are calculated using the rainfall and snowfall algorithms for the entire time series following the procedures described in Sections 2.3 and 2.4 (Fig. 6b and c). Ancillary data provided by the ship operator or the onboard weather service comprise NAV files with date, time, longitude and latitude with at least minute resolution along with routine surface meteorological measurements (MET) that store data in minute intervals (e.g. through the DSHIP system for German R/V's, http://www.bsh.de/) with a varying number of meteorological and oceanographic parameters that at least include the date, time, air temperature, relative and absolute wind speed and direction, surface pressure and humidity (Fig. 6e and f). Additionally, most ships provide three to six hourly logs of ship bridge weather observations stored in the WMO standard present weather (ww) and past weather W1 and W2 codes (SYN, Fig. 6g). The codes descriptions are available via http://www.wmo.int/pages/prog/www/ WMOCodes/Manual/Volume-I-selection/Sel2.pdf and are listed in Petty (1995). The times of all data sets are synchronized and stored in universal time (UT). The delivered data format is usually ASCII and occasionally binary code. During harbor maintenance or cruise-leg crew exchange times, the data is transferred.

The quality control and processing chain of these data streams, their collocation and the method to identify the precipitation phase is described in the following.

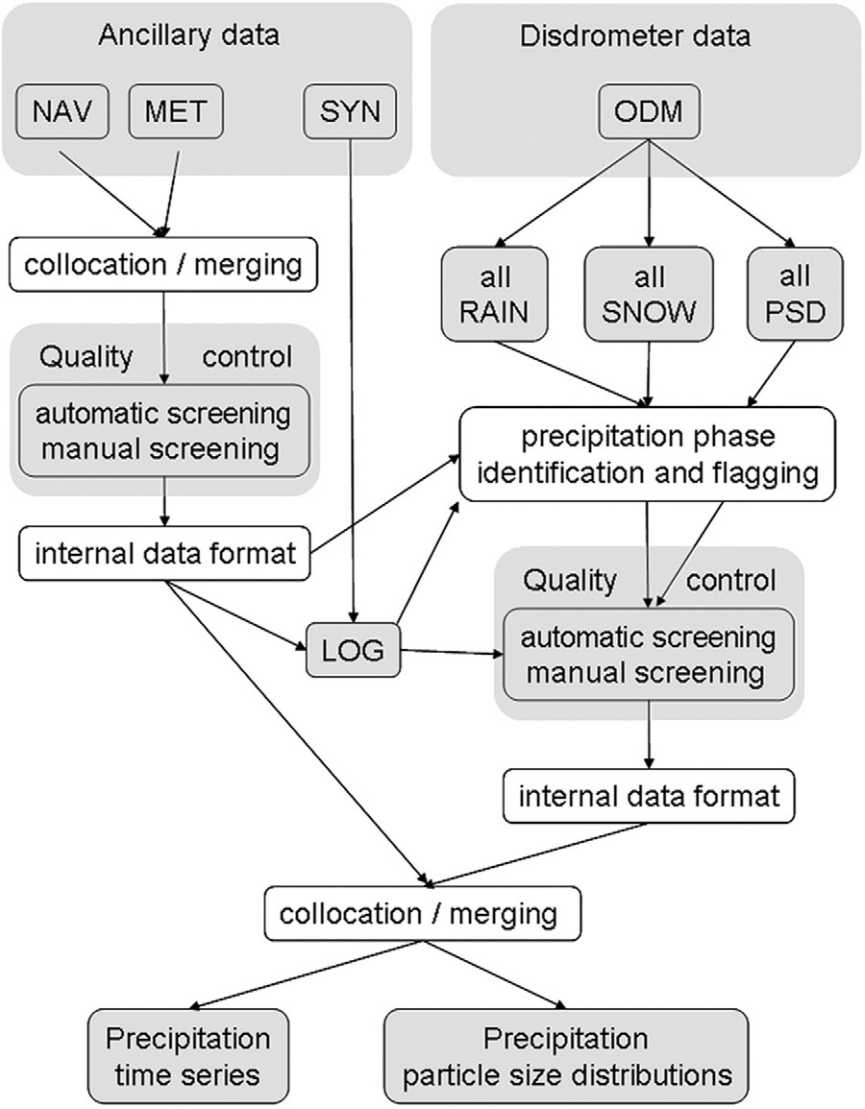

Fig. 5. Flow chart of the OceanRAIN data processing chain from the disdrometer and shipboard ancillary input data sets to precipitation products.

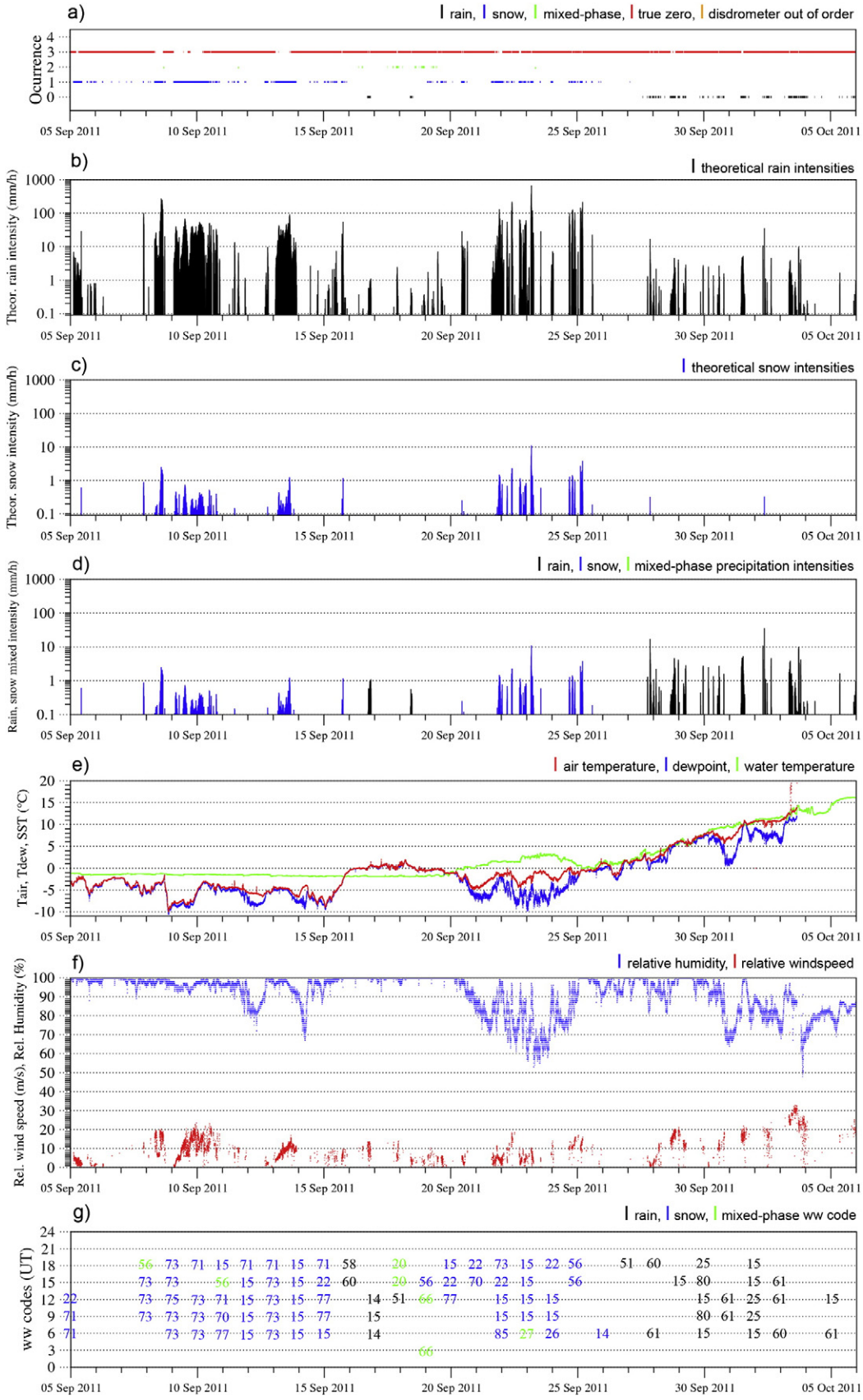

Fig. 6. Time series from R/V Polarstern between 05 September and 05 October 2011 in the Arctic Atlantic Ocean starting with a snow period that changes through mixed-phase into rainfall. Panel a) shows the occurrence of rain, snow, mixed-phase and true zeros. The numbers 0 to 4 correspond to the flag values in the data set. Panel b) contains the theoretical rain intensities on a log-y-axis scaled up to 1000 mm/h for identification of unrealistically high values. Panel c) shows the corresponding theoretical snow time series. Panel d) shows the actual time series. Furthermore, panel e) shows the air temperature, dewpoint and water temperature, f) the relative humidity and relative wind speed and g) the 3-hourly color-coded ww-codes used to identify the precipitation type periods.

4.3. Quality control

Data quality is significantly improved when monitoring of automated measurements is possible using onboard personnel who report problems to shore-side scientists (Smith and co-Authors, 2010). Therefore, within OceanRAIN, contacts are established to onboard personnel. Reported issues are in most cases solvable resulting only in minor data outages. Nonetheless, significant data outages already occurred resulting from errors caused by negligent handling or manipulation of the instruments, e.g., a drilled disdrometer cable or a piece of a fig found in the optical volume. During regular visits of the R/V's for data download, maintenance and exchange of the instruments, it is essential to discuss with the board crews and science members about special weather occurrences. This may comprise periods with icing or riming of sensors, extreme sea state with wave water up to the mast level or extreme precipitation events, observed problems or issues that occurred during the cruise. Additionally, metadata about changes in instrumentation, mounting positions or instrument failures is collected.

To ensure providing a consistently high quality database, all incoming data need to pass cascading quality control checks using automatic and manual screening procedures (Fig. 5). An automatic preprocessing applied to the temporally continuous ancillary data verifies the raw NAV and MET files for the existence of date, time, latitude and longitude, flagging non-sequential data and duplicate times. Data with non-correctable errors are identified and deleted from the final data record and missing data periods are logged. If ship navigational data or time is not available or could not be reconstructed from previous and following minutes by interpolation, all affected data is discarded. Additionally, the NAV data is graphically controlled for ship position, movement and speed. All arriving data is recorded in UT with synchronized clocks and is checked for consistency. In the next step, the collocated and merged NAV/MET data is automatically checked for out of range values and data plausibility. For example, the air temperature is checked for values within a range of ± 40 °C and to be greater than or equal to the dewpoint temperature. Sea-level pressure values are flagged if outside a range of 950 to 1050 hPa. The wind direction is inspected to be 0° for calm wind (0 m/s) and 360° for north wind (wind blowing from the North) with values greater than 0 m/s. Relative humidity is inspected to be within 0 and 100% and values beyond the upper bound are analyzed for dense fog or rime. Once the automatic preprocessing is complete, a visual inspection of time series using graphics and scatter plots is performed to verify or falsify the flagged data of the automatic preprocessor. This ensures that extreme values are either correctly accepted or rejected according to their occurrence within a realistic or unrealistic range of surrounding values in the time series. Erroneous, discontinuous or suspect data in the NAV/MET record are overwritten with −999 as a global missing value flag. The quality controlled NAV/MET data is converted into an internal data format for further processing (Section 4.4).

Metadata supplied by ship personnel are used to identify time periods with inoperative ODM470 instrumentation due to sensor malfunction, onboard instrument maintenance or meteorological extremes causing complete riming or icing of the disdrometer, anemometer or precipitation detector. Additionally interesting features, e.g. extreme weather situations or sea state, might be reported in the shipboard metadata and is valuable information documenting realistic extreme values. Satellite imagery is used as ancillary data if the meteorological situation is not well determined. Data from such periods enters the database only after careful inspection, or they might be discarded. Furthermore, the entire ODM precipitation time series is checked for values outside the realistic range by sequentially raising the thresholds to 50, 75 and 100 mm/h. Single minutes of discontinuous spikes in the precipitation records not belonging to a precipitation event (e.g. shower) can be identified as erroneous data and are rigorously excluded from the data records along with similarly unrealistic spikes in the ODM relative wind speed data (values > 40 m/s are internally flagged for further inspection). Such spikes are usually either electronically induced errors or occur when both instruments are on (IRSS88 and ODM470) and large objects (e.g. birds or a human hand) are blocking the optical volume.

Furthermore, the data is undergoing plausibility cross-checks to assure that the MET air temperature records and the SYN codes (through the LOG file; Section 4.4) are in agreement with the assigned precipitation phase of the ODM rain- and snowfall algorithm results. Contradicting data is flagged for further manual inspection.

4.4. Data processing

The data processing chain from the shipboard data sources described in Section 4.2 towards the final products is summarized in the flow chart of Fig. 5. In the first step of the processing chain, the temporally continuous NAV and MET data are collocated and merged into a common dataset at the highest possible temporal resolution, preferably minute data. If SYN codes are available, these are inspected for periods of observed rain, mixed-phase and snowfall and stored to a log file (LOG). The collocated NAV/MET data is visualized into time series records and checked for air temperature values to be consistent with the SYN log file information regarding the liquid, mixed-phase and solid precipitation periods. Based on this information, the LOG file is updated and discriminated into the precipitation phases containing date, time, air temperature, ww, W1, and W2. Precipitation flags are set to 0 for rain, 1 for snow and 2 for mixed-phase precipitation.

In the next step, the temporally discontinuous ODM data is calculated to provide preliminary minute resolution PSDs and precipitation time series by applying the rainfall algorithm (all-rain) and the snowfall algorithm (all-snow) to the entire data stream. Fig. 6 illustrates this procedure using the theoretical rain and theoretical snowfall time series in conjunction with the SYN data for one month (5 September 2011 to 5 October 2011) of R/V Polarstern data from the Arctic Ocean area of the North Atlantic. This time series example comprises the transition from a period with snowfall to rainfall intersected by mixed-phase precipitation. At this step of the processing chain the precipitation phase is still an unknown parameter. The preliminary all-rain time series of the ODM is inspected (Fig. 6b). Beside a realistic range of rainfall values during times coinciding with values flagged 0 for rainfall, this time series also contains different long phases ranging from minutes to weeks of out-of-range rainfall values with spikes continuously reaching between 200 and more than 1000 mm/h. Comparisons with the LOG file indicate that these unrealistic spikes coincide in most cases with time periods of snowfall. The solid particles of diameters beyond 6 mm are treated by the rainfall algorithm as huge drops generating unrealistically extreme rainfall. The period between the unrealistic spike onset and end turns out being an even more precise temporally-resolved measure for the precipitation phase change compared to the SYN data (Fig. 6g). This is because the SYN data usually provides observations in 3-hourly intervals on the synoptic hours while the minute-resolution ODM data determines the phase change precisely. Consequently, all real rainfall minutes receive their final flag 0 while all remaining precipitation minutes are replaced by the corresponding snow rate values and receive the preliminary flag 1 indicating snow. Vice versa, the snowfall algorithm precipitation intensities are mostly close to zero during rainfall periods and take on a realistic range of values only for real snow and mixed-phase events (Fig. 6c).

To date, there is no mixed-phase precipitation algorithm available that discriminates between the liquid and frozen fractions on the basis of the minute values. Nonetheless, it is important to distinguish between snow and mixed-phase events. Therefore, the assignment to mixed-phase with flag 2 is made when the LOG file based on the SYN information contains mixed-phase observations. If no SYN observations are available, the air temperature (Fig. 6e) and relative humidity information (Fig. 6f) along with the rainfall intensities (values of unrealistic spikes) serve as an indicator for mixed-phase precipitation. In most of these cases, the temperature varies between $+/-1.5$ °C. The peculiarity

for mixed-phase identification is that the rainfall data shows high values that are not as high as the ones observed for pure snow spectra, while the snow algorithm data yields unrealistically low results or may be zero (Fig. 6a, b and c). It is important to note that the mixed-phase precipitation intensities are less certain compared to the snow- and rainfall rates. As the snowfall algorithm is used to derive the mixed-phase precipitation, the mixed-phase intensities are biased low compared to the unknown true rate. This is because the liquid fraction of the precipitation is treated by the algorithm as solid particles. The underestimation of the precipitation rate increases with the amount of liquid droplets contributing to the PSD of the minute spectra. Overall, the uncertainties associated with mixed-phase precipitation rate estimates affect 17.5% of the precipitation events measured during two years onboard R/V 'Polarstern' (Section 5).

Finally the rain, snow and mixed-phase flagged ODM precipitation rates (Fig. 6a and d) and PSDs are collocated and merged with the NAV/MET data, resulting in a temporally discontinuous time series with minute resolution. Additionally, a temporally continuous time series is processed. This is done by including the true-zero precipitation measurements. True-zero values, flagged with the value 3, are assigned to all minutes with no precipitation occurrence, while the OceanRAIN instrumentation was operative. Flag 3 contains precipitation values of 0.00 mm/h while the ODM relative wind speed and reference voltage is set to missing value 888.88. Inoperative periods (disdrometer out of order or under maintenance) are allocated with flag 4 and precipitation, relative wind speed and reference voltage are set to 999.99. Data is provided while the ships are out at sea. Harbor times are assigned with flag 5. All precipitation ship data sets are lines of point measurements in time. The data sparseness relative to model data or areal measurements of satellites prevents direct constructions of gridded datasets. The output is written to standard ASCII files (including README files containing metadata) and netCDF format that contain the metadata in the self-describing file format. The metadata contains information about the sensors, their location, calibration, data formats and units. The file names contain the four digit ship call sign, the year, month and date of the first record in the file followed by a four digit value indicating the number of consecutive days and the data suffix.ascii or.nc. As an example, the data record from R/V 'Polarstern' would be DBLK.20100615.820.nc with measurements started on 15 June 2010 with a record of 820 continuous days excluding harbor times. The time series contains 26 parameters including date, time, latitude, longitude and 18 meteorological variables that are listed in Table 3.

Table 3
Description of 26 parameters included in the R/V 'Polarstern' precipitation time series.

Parameter	Unit or value range	Source
Line count	[]	Calculated
Date	DDMMYYYY	Common to all
Time	HHMM [UT]	Common to all
Minute of the day	1–1400	Calculated
Continuous count	seconds since 01.06.10 00UT	Calculated
Latitude	−90° to 90°	NAV
Longitude	−180° to 180°	NAV
Air temperature	°C	MET
Dew point temperature	°C	MET
Water temperature at −5 m	°C	MET
Relative humidity	%	MET
Sea-level pressure	hPa	MET
Relative wind speed	m/s	MET
Relative wind direction	deg	MET
Absolute wind speed	m/s	MET
Absolute wind direction	deg	MET
Global radiation	W/m^2	MET
Direct radiation	W/m^2	MET
Horizontal visibility	m	MET
Low cloud base height	m	MET
Maximum wind speed	m/s	MET
Ship rain gauge	mm/h	MET
Precipitation rate	mm/h	ODM
Relative wind speed	m/s	ODM
Reference voltage	V	ODM
Precipitation flag	0 = rain, 1 = snow, 2 = mixed, 3 = true zero, 4 = inoperative, 5 = harbor time	Calculated

5. Measurement examples and results

Examples of the resulting data sets are visualized for a 27-month time period onboard R/V 'Polarstern' comprising the entire time record of the OceanRAIN deployment from 10 June 2010 to 07 October 2012. Fig. 7 shows the Atlantic Ocean track of R/V 'Polarstern' from its base in Bremerhaven, Germany to the polar regions. The cruises comprise scientific missions and supply cruises for the Antarctic Georg von Neumayer station that are documented in detail at http://www.awi.de/en/infrastructure/ships/polarstern/. The tracks are visualized discontinuously as only navigational data with precipitation occurrence are plotted. The color-coding represents rainfall occurrence in black, snowfall in blue and mixed-phase precipitation in green. It is noteworthy that R/V 'Polarstern' crossed directly over the North Pole from 20 to 23 August 2011 during the northern hemispheric late summer season. The transects through the Atlantic Ocean also offer the opportunity of measuring precipitation in the mid-latitudes including the Southern Oceans, the subtropics and the ITCZ. Fig. 7 additionally shows the precipitation track of the Russian R/V 'Akademik Ioffe' in red for the time period from 3 September 2010 to 28 May 2013 comprising 33 months of data.

The color-coded R/V 'Polarstern' precipitation track of Fig. 7 is visualized into a continuous time series in Fig. 8. Between 10 June 2010 and 07 October 2012 a total of 1.091.876 min of data with 26 parameters were recorded excluding harbor times (Tab. 3). Precipitation occurred in 10.4% of the time with a total of 113,716 min. Fig. 8a shows the precipitation occurrence using the flags in the database: 0 = rainfall, 1 = snowfall, 2 =mixed-phase, 3 = true zero, 4 = disdrometer out of order. A total of 54,607 min contained rainfall (Fig. 8b, black) resulting in a total occurrence of 5.0% and a relative occurrence of 48.0%. In total, 39,221 min of snowfall (Fig. 8b, blue) occurred in 3.6% of the time or 34.5% relative to the precipitation occurrence. Mixed-phase precipitation (Fig. 8b, green) occurred in 19,888 min with 1.8% of the time, equivalent to 17.5% of the precipitation occurrence. Within this time period, a total precipitation accumulation of about 1000 mm was recorded, of which 88.2% was rain, 8.4% snow and 3.4% mixed-phase. The ratio of the sampled rain, snow and mixed-phase precipitation depends on the ship's track and is biased towards solid precipitation, as the target area of R/V 'Polarstern' is the high-latitudes.

Additionally, Fig. 8c illustrates the air temperature in red, the dewpoint temperature in blue, and the water temperature at 5 m depth in green. The relative wind speed is shown in red and the relative humidity in blue in Fig. 8d. The mean sea-level pressure is documented in Fig. 8e. Fig. 8 is plotted temporally continuous, with 89.6% of the precipitation occurrence being true-zero values (red line in Fig. 8a). The line is intersected by white areas indicating harbor times with no data. The time series repeatedly shows periods of intense rainfall that coincide with transects through the ITCZ and passages of mid-latitude cyclones (Fig. 8b). Extreme precipitation with minute values greater

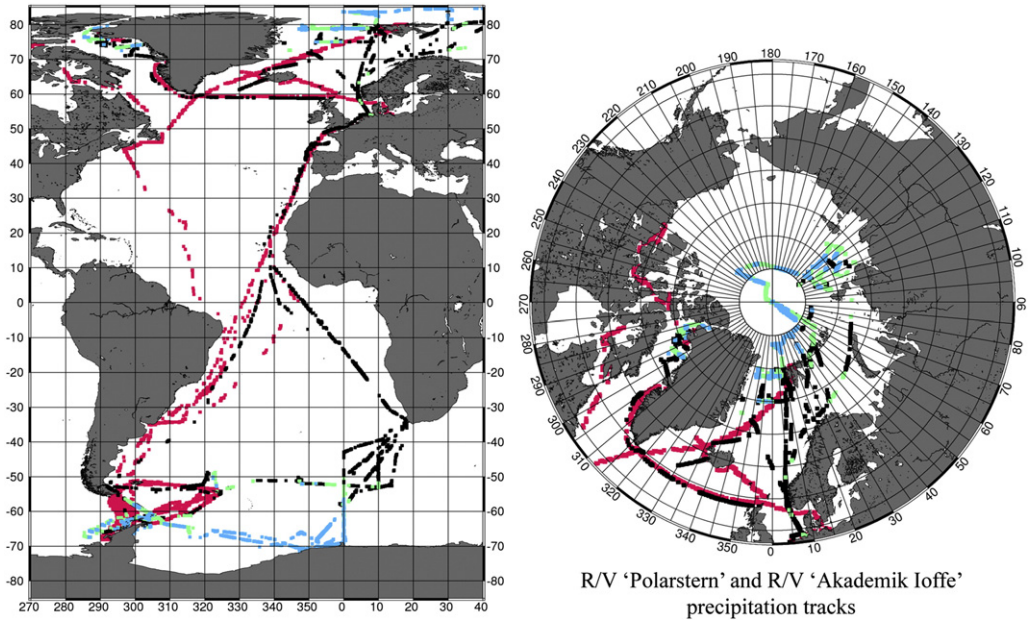

Fig. 7. Four years of precipitation tracks (precipitation occurrence only) of R/V 'Akademik Ioffe' (9/2010 to 9/2012) in red and R/V 'Polarstern' (6/2010 to 10/2012) in color-coding, indicating rainfall in red, snowfall in blue and mixed-phase precipitation in green for the entire Atlantic Ocean (left) and the northern hemisphere (right). Note the crossing of R/V 'Polarstern' directly over the North Pole.

than 50 mm/h are recorded during 27 min. 17 min belong to tropical ITCZ precipitation events including the largest recorded rainfall intensity of 113.7 mm/h. It is remarkable that 10 min with extreme precipitation occurred in post-frontal mid-latitude shower systems, with the highest value being 91.0 mm/h. The most intense snowfall event occurred at 88°N, with a snow intensity of 12.2 mm/h. The largest mixed-phase precipitation minute value occurred at 62°S with 15.6 mm/h. Convective rainfall defined by values greater than 5 mm/h after Houze (1993) occurred in 0.1% of the time but accounts for 52% of the rain accumulation.

The PSDs for the 27 continuous measurement months onboard R/V 'Polarstern' visualized in Fig. 7 and 8 are shown in Fig. 9. The upper left panel illustrates the distributions for 54,607 min of rainfall, the upper right panel for 39,221 min of snowfall, and the lower left panel shows 19,888 min of mixed-phase precipitation. In each of these panels, the dots indicate the integrated number of particles N(bin) of Eq. (2). The triangles show the integrated normalized number of particles to account for the non-constant interval width of the logarithmic size binning. The numerous point values denote the spread of the individual minute-based number concentrations. Finally, the average number concentration is plotted as stars and contains the sum of the individual minute spectra divided by the total number of spectra. Consequently, it falls off rapidly at larger bin sizes, as these infrequently contain data compared to the small bin sizes which almost always contain data (Section 2.4). In the lower right panel of Fig. 9, the three averaged number concentration curves are summarized for comparison with open circles for rainfall, stars for snowfall, and triangles for mixed-phase precipitation. Individual minute data may have a larger random error compared to the representative statistics of the averaged number concentrations. The rainfall number concentration exhibits its maximum of 485 particles at the smallest recordable particle diameters of 0.43 mm and falls off steeply towards the largest drops with diameters of about 6.6 mm. The snowfall number concentration curve peaks with 827 particles at a diameter of 0.69 mm. The slope of the curve is small compared to rainfall. Largest snowflakes reach a diameter of about 11.6 mm. The mixed-phased precipitation curve peaks as rainfall at 0.43 mm with 421 particles. For small particles, the slope is similar to that of rainfall. For particles between 1 to 7 mm in diameter, the curve shows a slope similar to snowfall. The curve intersects with the snowfall curve at 8 mm diameter, indicating that mixed-phased precipitation contains larger snowflake aggregates more frequently. The largest particles reach a diameter of 13.6 mm. In total, solid particles occur more frequently than liquid particles. Liquid droplets are more prone to evaporation compared to solid particles. Additionally, large drops tend to break apart into numerous droplets.

By October 2014, the continuously growing data set from all available ships comprises more than 370,000 min of precipitation with about 3.7 million measurement minutes.

6. Conclusions and outlook

OceanRAIN is to date the only disdrometer-based long-term systematic oceanic shipboard precipitation data collection effort for surface validation of satellite, re-analysis and model data. The mainstay of the measurements is the automated ODM470 disdrometer. In combination with the IRSS88 precipitation detector and the cup anemometer, it is a unique system based on robust hardware with minimal maintenance requirements that enables a complex measurement task: the estimation of rain and snow intensities through PSDs onboard moving ships under high wind speeds and rough sea state. The selected research ships transect all climate related hotspots over the global oceans, including the Arctic and Antarctic Oceans, the Southern Ocean, the mid-latitudes, the subtropics and the ITCZ. The cruises also comprise the cold-season high-latitudes in addition to the usual research ship cruises to the polar regions during summertime.

The rain- and snowfall algorithms are applied to the collected ODM470 data, and PSDs are calculated in minute resolution. Rigorous hardware calibration and rainfall verification procedures guarantee high quality of the measurements. A data processing chain has been implemented for the ingest of different incoming shipboard data streams, their automatic and visual quality control. Identification and flagging procedures for the precipitation phase along with collocation and merging of the ODM470 and ancillary data streams into the products were developed. Temporally discontinuous and continuous precipitation time series and PSDs distinct for rain, snow and mixed-phase precipitation are constructed. Data products comprise precipitation occurrence, intensity and accumulations.

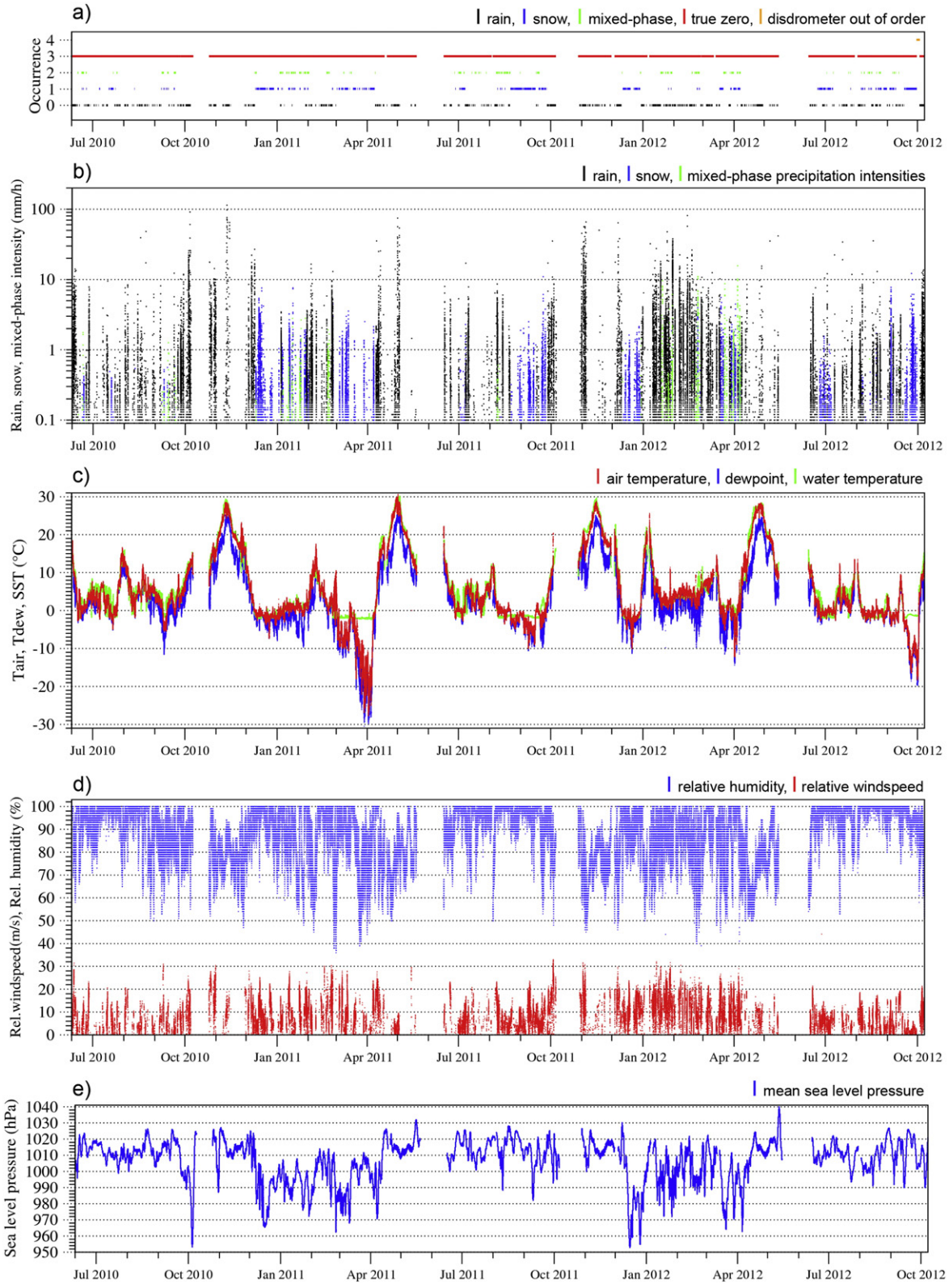

Fig. 8. Two years of R/V 'Polarstern' from June 2010 to 07 October 2012 covering all latitudes of the Atlantic Ocean. Panel a) shows the precipitation occurrence using the data flag values: 0 = rain, 1 = snow, 2 = mixed-phase, 3 = true zero (no precipitation), 4 = disdrometer out of order. The remaining white sections refer to harbor times were no data is recorded. Panel b) contains the precipitation intensities for rain (black, 54,607 min), snow (blue, 39,221 min) and mixed-phase (green, 19,888 min) in mm/h. Panel c) shows the air temperature (red), dewpoint (blue) and water temperature (green). Panel d) contains the relative humidity (blue) and the relative wind speed (red). Panel e) visualizes the mean sea-level pressure.

By October 2014, the steadily growing database contained more than 3.7 million minutes of precipitation (including true-zero values) from eight ships covering all climatic regions. In absolute numbers, precipitation occurs in about 10.4% of the time with 5.0% rain, 3.6% snow, and 1.8% mixed-phase. Convective rainfall occurs in 0.1% of the time but accounts for 52% of the rain volume.

Especially the new satellite generations of GPM, providing 3-hourly fields of global precipitation, SSMIS and MeghaTropiques may benefit

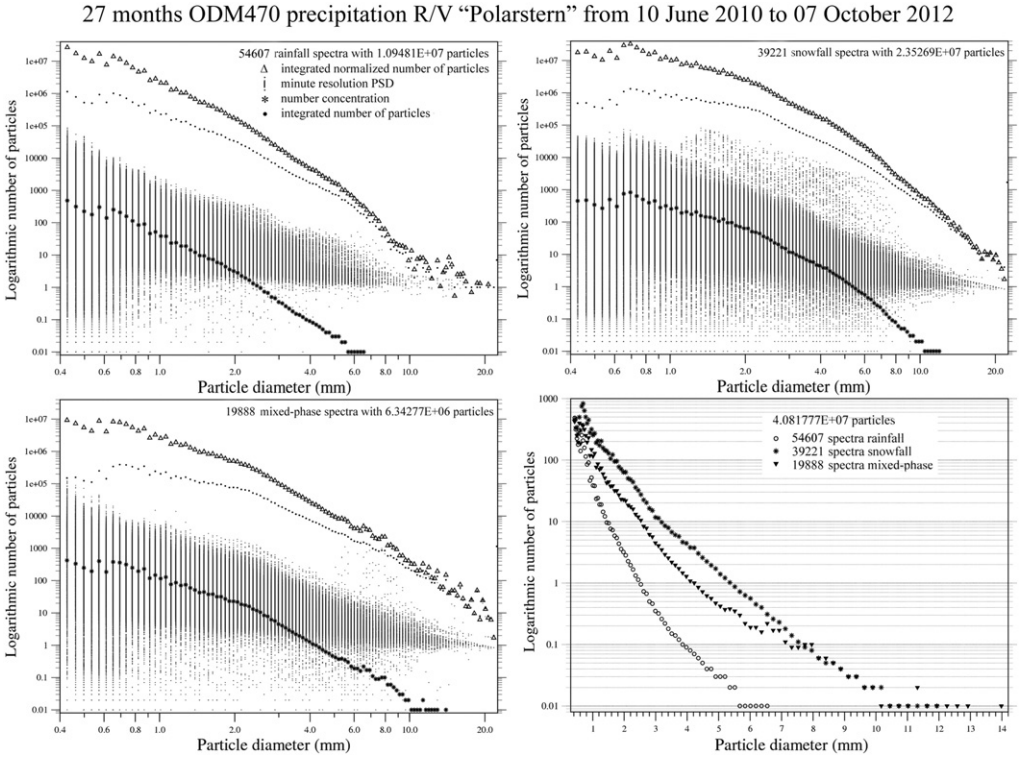

Fig. 9. Particle size distributions for 27 months of R/V 'Polarstern' using the same data as in Fig. 7 for 54,607 spectra of rainfall (top left panel), 39,221 spectra of snowfall (top right panel), and 19,888 spectra of mixed-phase precipitation (bottom left panel). The triangles shows the integrated normalized number of particles, the dots give the integrated number of particles, the bars indicate the spread of the individual minute resolution spectra, and the stars denote the number concentration. The number concentrations for all three precipitation phases are summarized in the bottom right panel.

from this surface reference data to accurately characterize rain and snow throughout many different types of precipitating systems and regions. The data also allows investigation of the point-to-area problem which arises from the surface point measurements and satellite areal footprints. Through the provision of minute-resolution precipitation time series and PSDs for the precipitation type rain, snow and mixed-phase, the database is suitable to constrain satellite retrievals and to investigate precipitation statistics, both globally and for specific regions or seasons. Furthermore, process studies of precipitation events reveal detailed insight into the microphysical processes of precipitation formation (e.g. cyclones or tropical convective showers) and document the occurrence of extreme events.

A large fraction of the precipitation measured is very light precipitation that is especially difficult to be measured by passive microwave satellites. In contrast, a large fraction of the Cloudsat CPR precipitation is very light precipitation. Consequently, validation between OceanRAIN and Cloudsat data may reveal insight into determining the fraction of virga-precipitation. Future tasks comprise automated procedures for deriving the precipitation phase based on PSD parameters and fall velocity values. Consequently, a separation scheme between the liquid and solid fraction for minute data PSDs is a prerequisite for the development of a mixed-phase algorithm.

Information on OceanRAIN including data products is available via http://www.oceanrain.org. The project is constantly seeking opportunities to increase the number of research and merchant ships involved.

Acknowledgments

Without the ship operators' support for instrument deployment, data delivery and remote communication the measurements, being the mainstay of this project, it would not have been possible: Irish Marine Institute, Norwegian Coast Guard (Kystvakten), Russian P.P. Shirshov Institute of Oceanology, Finnish Meteorological Institute and the German institutes and shipping companies Alfred Wegener Institute, Marum, Partenreederei MS Sonne, Brise Research, Control Station German Research Vessels at the University of Hamburg and Bundesamt für Seeschifffahrt und Hydrographie. The essential contributions of all unnamed colleagues and ship personnel are explicitly acknowledged. The author is especially grateful to the teams of Eigenbrodt and Mabanaft. Special thanks go to Dr. Stephan Bakan, Andrea Dahl, Olaf Dahl, Carsten Benecke, Tanja Thiele, Nicole Albern, Dr. Karl Bumke, Dr. Axel Andersson and Dr. Mark Carson. One of the reviewers is thanked for the numerous very helpful comments.

The project is funded by Mabanaft-Initiative Pro Klima, CliSAP/CEN, University of Hamburg, and the Max Planck Society (MPG).

References

Adler, R.F., Gu, G., Huffman, G.J., 2012. Estimating climatological bias errors for the global precipitation climatology project (GPCP). J. Appl. Meteorol. Climatol. 51, 84–99. http://dx.doi.org/10.1175/JAMC-D-11-052.1.

Anagnostou, E.N., Krajewski, W.F., Smith, J., 1999. Uncertainty quantification of mean-areal radar-rainfall estimates. J. Atmos. Ocean. Technol. 16, 206–215.

Andersson, A., Fennig, K., Klepp, C., Bakan, S., Graßl, H., Schulz, J., 2010. The Hamburg ocean atmosphere parameters and fluxes from satellite data — HOAPS-3. Earth Syst. Sci. Data 2, 215–234. http://dx.doi.org/10.5194/essd-2-215-2010.

Andersson, A., Klepp, C., Fennig, K., Bakan, S., Graßl, H., Schulz, J., 2011. Evaluation of HOAPS-3 ocean surface freshwater flux components. J. Appl. Meteorol. Climatol. 50, 379–398. http://dx.doi.org/10.1175/2010JAMC2341.1.

Atlas, D., Ulbrich, C., 1974. The physical basis for attenuation-rainfall relationships and the measurement of rainfall parameters by combined attenuation and radar methods. J. Rech. Atmosph. 275–298.

Béranger, K., Barnier, B., Gulev, S., Crepon, M., 2006. Comparing 20 years of precipitation estimates from different sources over the world ocean. Ocean Dyn. 56, 104–138.

Berry, D.I., Kent, E.C., 2011. Air–sea fluxes from ICOADS: the construction of a new gridded dataset with uncertainty estimates. Int. J. Climatol. 31, 987–1001. http://dx.doi.org/10.1002/joc.2059.

Bourlès, B., Co-Authors, 2008. The Pirata program: history, accomplishments, and future directions. Bull. Am. Meteorol. Soc. 89, 1111–1125. http://dx.doi.org/10.1175/2008BAMS2462.1.

Bradley, F., Fairall, C., 2007. A Guide to Making Climate Quality Meteorological and Flux Measurements at Sea. NOAA Technical Memorandum OAR PSD-311, NOAA/ESRL/PSD, Boulder, CO (108 pp.).

Bradley, S.G., Stow, C.D., Lynch-Blosse, C.A., 2000. Measurements of rainfall properties using long optical path imaging. J. Atmos. Ocean. Technol. 17, 761–772.

Brandes, E.A., Ikeda, K., Zhang, G., Schönhuber, M., Rasmussen, R.M., 2007. A statistical and physical description of hydrometeor distributions in Colorado snowstorms using a video disdrometer. J. Appl. Meteorol. Climatol. 46 (5), 634–650.

Bringi, V.N., Chandrasekar, V., 2001. Polarimetric Doppler Weather Radar: Principles and Applications. Cambridge University Press (636 pp.).

Brümmer, B., Müller, G., Klepp, C., Spreen, G., Romeiser, R., et al., 2010. Characteristics and impact of a gale-force storm field over the Norwegian Sea. Tellus 62A, 481–496. http://dx.doi.org/10.1111/j.1600-0870.2010.00448.x.

Bumke, K., Seltmann, J., 2011. Analysis of Measured Drop Size Spectra over Land and Sea. ISRN Meteorol. 2012 (Article ID 296575), 1–10. http://dx.doi.org/10.5402/2012/296575.

Bumke, K., Clemens, M., Grassl., H., Pang, S., Peters, G., co-authors., 2004. Accurate areal precipitation measurements over the land and sea (APOLAS). Baltex Newsl. 6, 9–13.

Bumke, K., Fennig, K., Strehz, A., Mecking, R., Schröder, M., 2012. HOAPS precipitation validation with ship borne rain gauge measurements over the Baltic Sea. Tellus A 64, 18486. http://dx.doi.org/10.3402/tellusa.v64i0.18486.

Clemens, M., 2002. Machbarkeitsstudie zur räumlichen Niederschlagsanalyse aus Schiffsmessungen über der Ostsee. PhD thesis, Christian-Albrechts-Universität, Kiel (178 pp.).

Curry, J.A., Coauthors, 2004. SEAFLUX. Bull. Am. Meteorol. Soc. 85, 409–424. http://dx.doi.org/10.1175/BAMS-85-3-409.

da Silva, A.M., Young, C.C., Levitus, S., 1994. Atlas of surface marine data 1994, Volume 1: algorithms and procedures. NOAA Atlas NESDIS 6. U.S. Department of Commerce, NOAA, NESDIS.

Ellis, T.D., L'Ecuyer, T.S., Haynes, J.M., Stephens, G.L., 2009. How often does it rain over the global oceans? The perspective from CloudSat. Geophys. Res. Lett. 36, L03815.

Fairall, C., Co-authors, 2010. Observations to quantify air sea fluxes and their role in climate variability and predictability. In: Hall, J., Harrison, D.E., Stammer, D. (Eds.), Proceedings of OceanObs'09: Sustained Ocean Observations and Information for Society. vol. 2. ESA Publication WPP-306, Venice, Italy, pp. 21–25. http://dx.doi.org/10.5270/OceanObs09.cwp.27, 299-313 (September 2009).

Frasson, R.P.M., Cunha, L.K., Krajewski, W.F., 2011. Assessment of the Thies optical disdrometer performance. Atmos. Res. (ISSN: 0169-8095) 101 (1–2), 237–255. http://dx.doi.org/10.1016/j.atmosres.2011.02.014.

Großklaus, M., 1996. Niederschlagsmessung auf dem Ozean von fahrenden Schiffen. PhD thesis. Institut für Meereskunde an der Christian-Albrechts-Universität, Kiel.

Großklaus, M., Uhlig, K., Hasse, L., 1998. An optical disdrometer for use in high wind speeds. J. Atmos. Ocean. Technol. 15, 1051–1059.

Hasse, L., Großklaus, M., Uhlig, K., Timm, P., 1998. A ship rain gauge for use under high wind speeds. J. Atmos. Ocean. Technol. 15, 380–386.

Hayes, S., Mangum, L., Picaut, J., Sumi, A., Takeuchi, K., 1991. TOGA-TAO: a moored array for real-time measurements in the tropical Pacific Ocean. J. Geophys. Res. 72, 339–347.

Hogan, A., 1994. Objective estimates of airborne snow properties. J. Atmos. Ocean. Technol. 11, 432–444.

Hou, Arthur Y., Kakar, Ramesh K., Neeck, Steven, Azarbarzin, Ardeshir A., Kummerow, Christian D., Kojima, Masahiro, Oki, Riko, Nakamura, Kenji, Iguchi, Toshio, 2014. The global precipitation measurement mission. Bull. Am. Meteor. Soc. 95, 701–722. http://dx.doi.org/10.1175/BAMS-D-13-00164.1.

Houze Jr., R.A., 1993. Cloud Dynamics. Academic Press, San Diego (573 pp.).

Huffman, G.J., Co-authors, 1997. The global precipitation climatology project (GPCP) combined precipitation dataset. Bull. Am. Meteorol. Soc. 78, 5–20.

Huffman, G.J., Co-authors, 2007. The TRMM multisatellite precipitation analysis (TMPA): quasi-global, multiyear, combined-sensor precipitation estimates at fine scales. J. Hydrometeorol. 8, 38–55.

Huffman, G.J., Klepp, C., 2011. Meeting summary: fifth workshop of the International Precipitation Working Group. Bull. Am. Meteorol. Soc. http://dx.doi.org/10.1175/BAMS-D-11-00030.1.

Illingworth, A., Stevens, C., 1987. An optical disdrometer for the measurement of raindrop size spectra in windy conditions. J. Atmos. Ocean. Technol. 4, 411–421.

IPCC, 2013. Climate change 2013: the physical science basis. In: Stocker, T.F., Qin, D., Plattner, G.-K., Tignor, M., Allen, S.K., Boschung, J., Nauels, A., Xia, Y., Bex, V., Midgley, P.M. (Eds.), Contribution of Working Group I to the Fifth Assessment Report of the Intergovernmental Panel on Climate Change. Cambridge University Press, Cambridge, United Kingdom and New York, NY, USA (in press).

Josey, S.A., Kent, E.C., Taylor, P.K., 1998. The Southampton Oceanography Centre (SOC) Ocean–Atmosphere Heat, Momentum and Freshwater Flux Atlas. Southampton Oceanography Centre Rep.6, Southampton, United Kingdom (30 pp.).

Kent, E., co-authors, 2010. The voluntary observing ship (VOS) scheme. In: Hall, J., Harrison, D.E., Stammer, D. (Eds.), Proceedings of OceanObs'09: Sustained Ocean Observations and Information for Society. vol. 2. ESA Publication WPP-306, Venice, Italy, pp. 21–25. http://dx.doi.org/10.5270/OceanObs09.cwp.48, 551-561 (September 2009).

Kidd, C., Huffman, G.J., 2011. Review global precipitation measurement. Meteorol. Appl. 18, 334–353. http://dx.doi.org/10.1002/met.284.

Klepp, C., Bumke, K., Bakan, S., Bauer, P., 2010. Ground validation of oceanic snowfall detection in satellite climatologies during LOFZY. Tellus A 62 (4), 469–480. http://dx.doi.org/10.1111/j.1600-0870.2010.00459.x.

Kummerow, C., Hong, Y., Olson, W.S., Yang, S., Adler, R.F., co-authors, 2001. The evolution of the Goddard Profiling Algorithm (GPROF) for rainfall estimation from passive microwave sensors. J. Appl. Meteorol. 40, 1801–1820.

Lanza, L.G., Vuerich, E., 2009. The WMO field intercomparison of rain intensity gauges. Atmos. Res. 94 (4), 534–543.

Lempio, G., 2006. Machbarkeitsstudie zur Messung festen Niederschlags mit dem Optischen Disdrometer. PhD thesis, Institut für Meereskunde an der Christian-Albrechts-Universität, Kiel (130 pp.).

Lempio, G., Bumke, K., Macke, A., 2007. Measurement of solid precipitation with an optical disdrometer. Adv. Geosci. 10, 91–97.

Levizzani, V., Laviola, S., Cattani, E., 2011. Detection and measurement of snowfall from space. Remote Sens. 3, 145–166.

Macke, A., Francis, P.N., Mc Farquhar, G.M., Kinne, S., 1998. The role of ice particle shapes and size distributions in the single scattering properties of cirrus clouds. J. Atmos. Sci. 55 (17), 2874–2883.

Marshall, J., Dobson, F., Moore, K., Rhines, P., Visbeck, M., co-authors, 1998. The Labrador Sea deep convection experiment. Bull. Am. Meteorol. Soc. 79, 2033–2058.

Michaelides, S. (Ed.), 2008. Precipitation: Advances in Measurement, Estimation and Prediction. Springer. ISBN: 978-3-540-77654-3 (540 pp.).

Mitrescu, C., L'Ecuyer, T., Haynes, J., Miller, S., Turk, J., 2010. CloudSat precipitation profiling algorithm — model description. J. Appl. Meteorol. Climatol. 49, 991–1003. http://dx.doi.org/10.1175/2009JAMC2181.1.

Oki, T., 1999. In: Browning, K.A., Gurney, R.J. (Eds.), The Global Water Cycle. Global Energy and Water Cycles. Cambridge, University Press, pp. 10–29.

Peterson, T.C., Easterling, D.R., Karl, T.R., Groisman, P., Nicholls, N., Plummer, N., Torok, S., Auer, I., Boehm, R., Gullett, D., Vincent, L., Heino, R., Tuomenvirta, H., Mestre, O., Szentimrey, T., Salinger, J., Forland, E.J., Hanssen-Bauer, I., Alexandersson, H., Jones, P., Parker, D., 1998. Homogeneity adjustments of in situ atmospheric climate data: a review. Int. J. Climatol. 18, 1493–1517.

Petty, G.W., 1995. Frequencies and characteristics of global oceanic precipitation from shipboard present-weather reports. Bull. Am. Meteorol. Soc. 76, 1593–1616. http://dx.doi.org/10.1175/1520-0477(1995)076<1593:FACOGO>2.0.CO;2.

Petty, G.W., 1997. An inter-comparison of oceanic precipitation frequencies from 10 special sensor microwave/imager rain rate algorithms and shipboard present weather reports. J. Geophys. Res. 102, 1757–1777.

Post, M.J., co-authors, 1998. The combined sensor program: an air–sea science mission in the central and western Pacific Ocean. Bull. Am. Meteorol. Soc. 78, 2797–2815.

Pruppacher, H.R., Klett, J.D., 1978. In: Reidel, D. (Ed.), Microphysics of Clouds and Precipitation. Springer. ISBN: 978-0792342113 (976 pp.).

Reed, R.K., Elliott, W.P., 1977. A comparison of oceanic precipitation measured by gage and assessed from weather reports. J. Appl. Meteorol. 16, 983–986.

Romanova, V., Köhl, A., Stammer, D., Klepp, C., Andersson, A., Bakan, S., 2010. Sea surface freshwater flux estimates from GECCO, HOAPS and NCEP. Tellus A 62 (4), 435–452. http://dx.doi.org/10.1111/j.1600-0870.2010.00447.x.

Rosenfeld, D., Ulbrich, C.W., 2003. Cloud microphysical properties, processes, and rainfall estimation opportunities. Radar and atmospheric science: a collection of essays in honor of David Atlas. Meteorol. Monogr. 52, 237–258 (Amer. Meteor. Soc.).

Schneider, U., Becker, A., Finger, P., Meyer-Christoffer, A., Ziese, M., Rudolf, B., 2013. GPCC's new land surface precipitation climatology based on quality-controlled in situ data and its role in quantifying the global water cycle. Theoret. Appl. Climatol.Global Precipitation Climatology Centre, Deutscher Wetterdienst, Offenbach, Germany http://dx.doi.org/10.1007/s00704-013-0860-x.

Send, U., co-authors, 2010. In: Hall, J., Harrison, D.E., Stammer, D. (Eds.), OceanSITES, In Proceedings of OceanObs'09: Sustained Ocean Observations and Information for Society (Vol. 2), Venice, Italy, 21–25 September 2009. vol. 2. ESA Publication WPP-306, pp. 913–922.

Smith, S., co-Authors, 2010. The data management system for the shipboard automated meteorological and oceanographic system (SAMOS) initiative. In: Hall, J., Harrison, D.E., Stammer, D. (Eds.), Proceedings of OceanObs'09: Sustained Ocean Observations and Information for Society (Vol. 2), Venice, Italy, 21 – 25 September 2009. vol. 2. ESA Publication WPP-306, pp. 959–968.

Stephens, G.L., Li, J.L., Wild, M., Clayson, C.A., Loeb, N., Kato, S., L'Ecuyer, T., Stackhouse, P.W., Andrews, T., 2012. An update on Earth's energy balance in light of the latest global observations. Nat. Geosci. 5, 691–696. http://dx.doi.org/10.1038/ngeo1580.

Taylor, P.K., 2000. Intercomparison and validation of ocean–atmosphere energy flux fields —final report of the Joint WCRP/SCOR Working Group on Air–Sea Fluxes. WCRP-112, WMO/TD-1036 (306 pp.).

Tokay, A., Kruger, A., Krajewski, W., 2001. Comparison of drop size distribution measurements by impact and optical disdrometers. J. Appl. Meteorol. 40, 2083–2097.

Trenberth, K.E., Fasullo, J.T., Kiehl, J., 2009. Earth's global energy budget. Bull. Am. Meteorol. Soc. 90, 311–323.

Weller, R.A., Bradley, E.F., Edson, J.B., Fairall, C.W., Brooks, I., Yelland, M.J., Pascal, R.W., 2008. Sensors for physical fluxes at the sea surface: energy, heat, water, salt. Ocean Sci. 4, 247–263.

Wijesekera, H.W., Rudnick, D.L., Paulson, C.A., Pierce, S.D., Pegau, W.S., Mickett, J., Gregg, M.C., 2005. Upper ocean heat and freshwater budgets in the eastern Pacific warm pool. J. Geophys. Res. 110. http://dx.doi.org/10.1029/2004JC002511.

Woodruff, S.D., et al., 2011. ICOADS release 2.5: extensions and enhancements to the surface marine meteorological archive. Int. J. Climatol. 31, 951–967. http://dx.doi.org/10.1002/joc.2103 (http://doi.wiley.com/10.1002/joc.2103).